

4-2018

Boron-Lined NaI Detector as An Efficient alternative To He-3 Neutrons Detectors

Amira Mostafa Gaber Emam

Follow this and additional works at: https://scholarworks.uaeu.ac.ae/phys_theses



Part of the [Physics Commons](#)

Recommended Citation

Emam, Amira Mostafa Gaber, "Boron-Lined NaI Detector as An Efficient alternative To He-3 Neutrons Detectors" (2018). *Physics Theses*. 4.

https://scholarworks.uaeu.ac.ae/phys_theses/4

This Thesis is brought to you for free and open access by the Physics at Scholarworks@UAEU. It has been accepted for inclusion in Physics Theses by an authorized administrator of Scholarworks@UAEU. For more information, please contact fadl.musa@uaeu.ac.ae.



جامعة الإمارات العربية المتحدة
United Arab Emirates University

United Arab Emirates University

College of Science

Department of Physics

BORON-LINED NaI DETECTOR AS AN EFFICIENT
ALTERNATIVE TO He-3 NEUTRONS DETECTORS

Amira Mostafa Gaber Emam

This thesis is submitted in partial fulfilment of the requirements for the degree of
Master of Science in Physics

Under the Supervision of Professor Mofreh R. Zaghloul

April 2018

UAEU Library

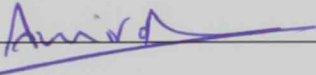


1000502021



Declaration of Original Work

I, Amira Mostafa Gaber Emam, the undersigned, a graduate student at the United Arab Emirates University (UAEU), and the author of this thesis entitled "*Boron-Lined NaI Detector as an Efficient Alternative to He-3 Neutrons Detectors*", hereby, solemnly declare that this thesis is my own original research work that has been done and prepared by me under the supervision of Professor Mofreh R. Zaghloul, in the College of Science at UAEU. This work has not previously been presented or published, or formed the basis for the award of any academic degree, diploma or a similar title at this or any other university. Any materials borrowed from other sources (whether published or unpublished) and relied upon or included in my thesis have been properly cited and acknowledged in accordance with appropriate academic conventions. I further declare that there is no potential conflict of interest with respect to the research, data collection, authorship, presentation and/or publication of this thesis.

Student's Signature: 

Date: 19/4/2018

Approval of the Master Thesis

This Master Thesis is approved by the following Examining Committee Members:

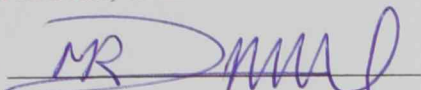
- 1) Advisor (Committee Chair): Mofreh R. Zaghloul

Title: Professor

Department of Physics

College of Science, UAEU

Signature



Date 19/4/2018

- 2) Member: Bashar A. Issa

Title: Professor

Department of Physics

College of Science, UAEU

Signature



Date

19/4/2018

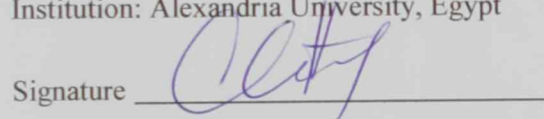
- 3) Member (External Examiner): Mohamed H. M. Hassan

Title: Associate Professor

Department of Nuclear Engineering

Institution: Alexandria University, Egypt

Signature



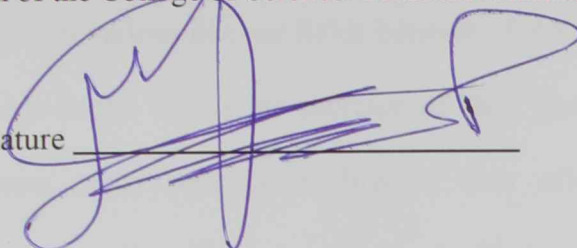
Date

20/4/2018

This Master Thesis is accepted by:

Dean of the College of Science: Professor Ahmed Murad

Signature

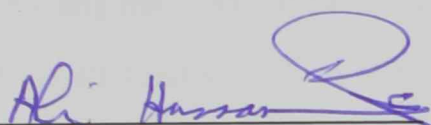


Date

16/5/2018

for Dean of the College of Graduate Studies: Professor Nagi T. Wakim

Signature



Date

16/5/2018

Copyright © 2018 Amira Mostafa Gaber Emam
All Rights Reserved

Advisory Committee

1) Advisor: Mofreh R. Zaghloul

Title: Professor

Department of Physics

College of Science

2) External Member: Walid A. Metwally

Title: Associate Professor

Department of Nuclear Engineering

Institution: University of Sharjah, UAE

Abstract

Helium-3 detectors are considered as the main component of most neutron detection systems in various nuclear fields because of their high thermal-neutron cross-section. But due to the worldwide shortage of He-3 gas after 2009 that led to a huge price increase, many researchers directed their efforts in order to find an efficient replacement. One of the proposed cost-effective alternatives is using an existing NaI detector covered with a thin layer of ^{10}B to detect the gamma rays emitted from excited ^7Li resulting from $^{10}\text{B}(n,\alpha)^7\text{Li}$ reaction. In this an MCNP model is developed to simulate He-3, BF₃ and boron-lined NaI detectors to simulate the response of each detector. Experimental measurements were made using the three detectors and compared to the simulation results for validation. The results show a good sensitivity when exposed to various neutron-flux distributions with a higher efficiency of boron-lined NaI than He-3 and BF₃ in addition to the ability to detect the gamma rays from the surrounding medium. The simulation and experimental results clearly demonstrate that boron-lined NaI detector is an efficient alternative for replacing He-3 detectors.

Keywords: Neutron detectors, boron-lined detectors, He-3 alternatives, MCNP.

Title and Abstract (in Arabic)

كاشف ايوديد الصوديوم المغطى بطبقة البورون كبديل فعال لكاشف الهيليوم-3 في الكشف عن النيوترونات

الملخص

تعتبر كاشفات الهيليوم-3 هي العنصر الأساسي لمعظم أنظمة الكشف عن النيوترونات في العديد من المجالات النووية ويرجع ذلك إلى القيمة المرتفعة للمقطع النيوتروني الكلي للنيوترونات الحرارية (thermal-neutron cross-section). نظراً للنقص في كمية غاز الهيليوم-3 على مستوى العالم بعد عام 2009 مما أدى إلى ارتفاع هائل في أسعار كاشفات الهيليوم-3 ، وجّه العديد من الباحثين جهودهم في سبيل إيجاد بديل فعال. ويعد استخدام كاشف ايوديد الصوديوم المغطى بطبقة رقيقة من البورون أحد أهم البدائل من حيث التكلفة وذلك عن طريق قياس اشعة جاما الناتجة من انحلال ${}^7\text{Li}$ الغير مستقر الناتج من التفاعل ${}^{10}\text{B}(n, \alpha){}^7\text{Li}$. في هذا البحث تمت مقارنة نتائج الاستجابة في الكشف عن النيوترونات بين كل من كاشف ايوديد الصوديوم المغطى بالبورون , كاشف الهيليوم-3 وكاشف ثلاثي فلوريد البورون من خلال عمل نموذج محاكاة باستخدام برنامج (MCNP). كما تم قياس الاستجابة مختبرياً ومقارنة النتائج مع نتائج القياس بالمحاكاة .

أظهرت نتائج المحاكاة والقياس المختبري حساسية جيدة لكاشف ايوديد الصوديوم المغطى بطبقة من البورون عند تغيير توزيع تدفق النيوترونات (neutron-flux distribution) وكفاءة أعلى من كل من كاشف الهيليوم-3 وكاشف ثلاثي فلوريد البورون هذا بالإضافة الي ميزة كاشف ايوديد الصوديوم المغطى بطبقة البورون في الكشف عن اشعة جاما من الوسط المحيط. أهم نتائج هذا البحث أن كاشف ايوديد الصوديوم المغطى بطبقة البورون يعتبر كبديل فعال لكاشف الهيليوم-3 في الكشف عن النيوترونات ويمكن استخدامه في العديد من التطبيقات.

مفاهيم البحث الرئيسية: الكشف عن النيوترونات - كاشفات البورون - بدائل كاشفات الهيليوم-3 - برنامج المحاكاة (MCNP).

Acknowledgements

First and foremost, I praise Allah for granting me this opportunity and providing me the capability to proceed successfully. I would like to thank, my mother who encouraged me to chase my dream again after giving up for many years. Thank you my father you were always and still the motivator of any achievement in my life.

I would like to express my sincere gratitude to Prof. Walid A. Metwally, for his patience, motivation, enthusiasm, and immense knowledge. His guidance helped me in all the time of research and writing of this thesis.

Also I am greatly appreciated and thankful to Prof. Mofreh Zaghloul who introduced me to the exciting field of Nuclear Physics.

My thanks and appreciation extends to Prof. Usama Al Khawaja for supporting me and to Prof. Salah Nasri who inspired me and added atmosphere of challenge every lecture of Quantum and Electromagnetism courses.

And I would like to thank laboratory team at Sharjah University, Eng. Samar El-Sayed, Eng. Ahmed Ababneh, Mr Osama Taqatqa, and Eng. Abdalla Habashy, for their help at experimental measurements.

Special thanks go to my Husband Sherif; his love, patience, help, and all the time support at ups and downs helped me along the way, YES, I can finish things. ☺

Dedication

To my beloved parents, my son Omar and my Husband Sherif

Table of Contents

Title	i
Declaration of Original Work	ii
Copyright	iii
Advisory Committee	iv
Approval of the Master Thesis	v
Abstract	vii
Title and Abstract (in Arabic)	viii
Acknowledgements	ix
Dedication	x
Table of Contents	xi
List of Tables.....	xiii
List of Figures	xiv
List of Abbreviations.....	xvi
Chapter 1: Introduction	1
1.1 Neutron Detection	1
1.2 Aims and Objectives	4
1.3 Relevant Literature	5
Chapter 2: Theory and Methods.....	7
2.1 Neutron Source.....	7
2.2 Detectors.....	8
2.2.1 NaI Detector	8
2.2.2 Description of Boron-Lined NaI Detector.....	11
2.2.3 BF ₃ Detectors.....	12
2.2.4 He-3 Detectors.....	14
2.3 Simulation	15
2.3.1 Surface Cards.....	18
2.3.2 Cell Cards	19
2.3.3 Materials	20
2.3.4 Tallies	22
2.3.5 Simulation Variables	23
2.4 Measurements.....	25
2.4.1 Detectors Specifications	25

2.4.2 Experiments.....	26
2.4.3 Experimental Setup	28
2.5 Net Counts and Error propagation.....	31
2.5.1 Sigma for MCNP Calculations	31
2.5.2 Sigma for Experiments Calculations	32
Chapter 3: Results and Discussions	34
3.1 Simulation Results.....	34
3.1.1 Effect of Adding Boron Layer to NaI Detector.....	35
3.1.2 Effect of HDPE Port Moderator Thickness.....	36
3.1.3 Effect of Detectors Distance from the Port	40
3.2 Experimental Results.....	43
Chapter 4: Conclusions	51
References	52
List of Publications	55
Appendix A: MCNP6 Input File	56
Appendix B: Simulation Results.....	61
Appendix C: Experimental Results.....	62

List of Tables

Table 1: Exothermic Reactions Used for Neutron Detection.....	1
Table 2: Materials Specification Used in MCNP.....	21
Table 3: Some Specifications of NaI, He-3 and BF ₃ Detectors.	25
Table 4: Adjustments for NaI Detector Response.	34
Table 5: MCNP Simulated Counts at Different Port Moderator Thickness for NaI and He3 detectors.	36
Table 6: MCNP Simulated Counts at Different HDPE Port Moderator Thickness for He-3 and BF ₃ Detectors.	38
Table 7: MCNP Simulated Counts in B-Lined NaI and He-3 Detectors at Different Distances from the Port.	40
Table 8: MCNP Simulated Counts in He-3 and BF ₃ Detectors at Different Distances from the Port.	40
Table 9: Photon Counts per Source Particles at Region of Interest from MCNP Simulation for NaI Detector with and without Boron Layer.	61
Table 10: Experimental Response of He-3 and B-lined NaI Detectors at Various HDPE Moderator Thicknesses.	62
Table 11: Experimental Neutron Response of BF ₃ and He-3 Detectors at Different HDPE Moderator Thicknesses.	62
Table 12: Experimental Neutron Response of B-Lined NaI and He-3 Detectors at Various Powers and Shifts.	63
Table 13: Experimental Neutron Response of BF ₃ and He-3 Detectors at Various Generator Powers and Distances from Port.....	64

List of Figures

Figure 1: Neutron Absorption Cross Sections for common materials Vs. Energy of Neutrons.....	3
Figure 2: Moderated & Shielded DD109.4 Neutrons-Generator at University of Sharjah.	8
Figure 3: Block Diagram of the Detection System of NaI Detector	9
Figure 4: Pulse Height Spectrum from a NaI(Tl) Scintillator for Gamma Rays Emitted by ^{60}Co	10
Figure 5: Boron Layer Covering NaI Detector	11
Figure 6: Interaction of Incident Neutrons with BF ₃ Gas.....	12
Figure 7: Typical Pulse Height Spectrum from BF ₃ Detector.....	13
Figure 8: Typical Pulse Height Spectrum for He-3 Detector.....	14
Figure 9: Particle History Example for Neutron Incident on Fissionable Block	16
Figure 10: DD Neutron Generator Setup with a) He-3 and Boron-Lined NaI Detectors. b) He-3 and BF ₃ Detectors.	17
Figure 11: XY Section of MCNP Generator Model Surfaces.....	18
Figure 12: YZ Section of MCNP Alignment Cells.....	19
Figure 13: a) HDPE Port Moderator Discs, b) Generator Front Port.....	27
Figure 14: He-3 and B-Lined NaI Detectors at 30 cm from the Neutrons Port.....	28
Figure 15: He-3 and BF ₃ Detectors at 50 cm from the Neutrons Port	28
Figure 16: Block Diagram of the Detectors and Neutron Generator	30
Figure 17: Simulated Pulse Height Spectrum of NaI Detector, with and without Boron Layer.	35
Figure 18: MCNP Simulated Net Counts in B-lined NaI and He-3 Detector at Different HDPE Moderator Thickness.	37
Figure 19: MCNP Simulated Net Counts in BF ₃ and He-3 detector at different HDPE Port Moderator Thicknesses.	39
Figure 20: MCNP Detector Response of B-lined NaI, He-3 at Various Distances from the Port.	41
Figure 21: MCNP Detector Response of He-3, BF ₃ at Various Distances from the Port.	42
Figure 22: Gamma Ray Spectrum in NaI detector, with and without Boron Layer	44
Figure 23: Experimental Net Counts in B-lined NaI and He-3 Detectors, Generator Power (2000 W).	45
Figure 24: Experimental Net Counts in He-3 and BF ₃ Detectors at Different HDPE Port Moderator Thickness.	46
Figure 25: Detector Response of B-lined NaI and He-3 detectors at Varying Neutron Generator Power and Fixed Distance at 30 cm from Port.	47

Figure 26: Detector Response of B-lined NaI and He-3 detectors at Varying Neutron Generator Power and Fixed Distance at 40 cm from Port.	48
Figure 27: Detector Response of B-lined NaI and He-3 Detectors at Varying Neutron Generator Power and Fixed Distance at 50 cm from Port.	48
Figure 28: Response of He-3 and Bf3 detectors at Varying Neutron Generator Power and at 30 cm from port.....	49
Figure 29: Response of He-3 and BF3 Detectors at Varying Neutron Generator Power and at 40 cm from Port.	50
Figure 30: Response of He-3 and Bf3 Detectors at Varying Neutron Generator Power and at 50 cm from Port.	50

List of Abbreviations

BPE	Borated Polyethylene
CPS	Counts Per Second
CPSP	Counts Per Source Particle
DD	Deuterium-Deuterium
GARR _n	Gamma Absolute Rejection Ratio for Neutrons
HDPE	High Density Poly Ethylene
MCNP	Monte Carlo N-Particle
NAA	Neutron Activation Analysis
PNNL	Pacific Northwest National Laboratory
RPMs	Radiation Portal Monitors

Chapter 1: Introduction

1.1 Neutron Detection

Neutrons are indirectly ionizing radiations, that are indirectly detected by interacting with matter and producing charged particles or photons, such as in (n, α), (n,p), (n, γ), or the (n,fission) reactions. Neutron detection is essential in a variety of different aspects of radiological applications such as research, nuclear reactors, and is indispensable in homeland security and safeguards. Thermal neutrons and fast neutrons, after being thermalized by moderator, can be detected via one of the most useful exothermic nuclear reactions shown in Table 1.

Table 1: Exothermic Reactions Used for Neutron Detection [1]

Reaction	Q Value (MeV)	Thermal Cross Section (barn)
$^3\text{He}(\text{n},\text{p})^3\text{H}$	0.765	5400
$^{10}\text{B}(\text{n},\alpha)^7\text{Li}$	2.79 (ground state)	3840
$^6\text{Li}(\text{n},\alpha)^3\text{H}$	4.78	937

Helium-3 is considered as the most suitable thermal neutron material due to several advantages such as high capture cross-section for thermal neutrons and negligible gamma ray sensitivity. Supply of ^3He is limited to production as a byproduct from the decay of ^3H (12.3-year half-life). Tritium was produced as part of weapons programs such as the Savannah River Site (SRS) in US, which was shut down due to safety concerns in 1988 and resulted in the elimination of the direct U.S. supply of ^3He . Helium-3 supply also existed from similar weapons activities in the

Russian Federation or as a byproduct of reactor operations such as Watts Bar and Sequoyah nuclear plants [2]. After September 11, 2001 a high request for ^3He detectors started to arise significantly for national security all over the world. The end of cold war led to the reduction in tritium production, which consequently led to a significant shortage of ^3He gas. The estimated yearly world demand and supply of ^3He is about (65000 l/y, 15000 l/y) respectively, which lead to the enormous price increase per liter from \$(40–85) by the end of 2008 to \$2500 for commercial use in 2012 [3].

As a result of the shortage and huge price increase of ^3He gas, exploring alternative methods for neutron detection became essential. Several programs have been developed and funded to find suitable alternative neutron detection methods [4].

It is desirable for a neutron absorber to have a large cross-section such that the interaction is likely to occur, and for the reaction products of the interaction to be highly energetic and easy to detect. As shown in Figure 1, both of ^{10}B and ^6Li show potential as ^3He replacements due to the relatively high cross section, ^{10}B (about 70% of that of ^3He) while ^6Li (about 18%). Boron-10 has high (n, α) reaction cross-section along the entire neutron energy spectrum. Boron-10 satisfies both requirements of high thermal neutron cross section and relatively high Q-value. With excellent gamma discrimination ^{10}B lined detectors could be ideal alternatives to ^3He detectors in applications with simultaneous high neutron and gamma flux [5].

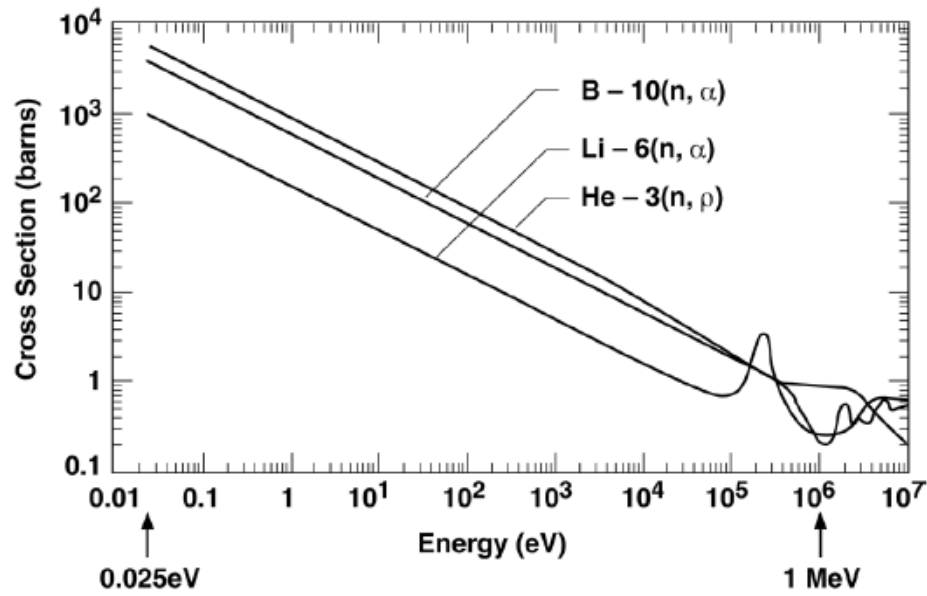
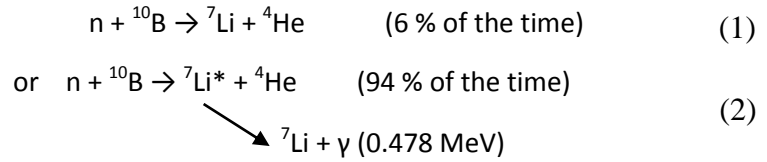


Figure 1: Neutron Absorption Cross Sections for common materials Vs. Energy of Neutrons [1]

The choice of ^{10}B was based on the comparison among the alternatives for ^3He summarized from Institute of Nuclear Materials Management (INMM) 52nd Annual meeting in 2011. In addition to the high cross section for thermal-neutrons absorption it is not expensive, no toxicity or degradation and possible for safeguards applications in radiation portal monitors (RPMs) [6].

1.2 Aims and Objectives

The objective of this work is to investigate a specific alternative detector for thermal neutrons that does not use ^3He by adding a thin layer of natural boron to the already existing NaI Scintillator γ -detector. The boron layer enabled the utilization of the nuclear reaction of thermal neutrons with boron nuclei with high cross-section (3840 barns) and emitting 0.478 MeV gamma rays from the decay of excited ^7Li according to the reactions



The emitted gamma with energy 0.478 MeV from the interaction can be detected by the enclosed NaI γ -detector.

To accomplish the above objective, we aim to model and simulate then experimentally test the boron-lined NaI detector and to compare the response in terms of efficiency and sensitivity with that of He-3 and BF3 detectors which are considered as the most efficient neutron detectors used up to date. The response will be determined for different neutron flux distributions with Monte Carlo simulation methods and the results will be validated through experimental measurements.

1.3 Relevant Literature

There have been many studies investigating the use of the promising isotopes ^{10}B and ^6Li [7-10]. A recent MCNP simulation study examined a simple model of (4"*4") NaI detector covered by thin layer of boron in neutron detection and a considerable efficiency was shown [11]. Also a boron-lined system has been tested as a possible alternative for neutron-detection technology for use in (RPMs) for national security applications and the absolute efficiency was found to be 24% above the required value (2.5 cps/ng) and the system was found to meet the requirements for neutrons-detection in a gamma ray field [12]. In [13], a hexagonal Boron-10 nitride (h- ^{10}BN) was used to construct a solid-state thermal-neutron detector as an alternative to He-3 detector. Results showed very narrow peaks of measured pulse-height spectra. In spite of the excellent gamma and neutron radiation discrimination, the neutron efficiency of the designed detector is limited by the h- ^{10}BN thickness and a thicker epilayers of h-BN was currently developed.

Adding ^{10}B to an existing α scintillator detector ZnS(Ag) has been tested early in 1955 as a feasible option to replace ^3He . Results showed low sensitivity to gamma rays and short time decay constant [14]. A group of researchers in 2016 [15], calculated the response and investigated the ability of using a commercial $^{10}\text{B}+\text{ZnS}(\text{Ag})$ neutron detector referred to as "nDet-Brick" N-15 detector as an alternative to He-3 detector in homeland security. The 24 and 48 mm front and back thickness of high density polyethylene (HDPE) respectively resulted in nearly linear response for the energy range ($10^{-7} - 1$ MeV). While for energies less than 10^{-2} Me, the best response was from a zero mm HDPE (i.e., bare detector).

A neutron detector system with a ^{10}B -lined tube was tested in comparison with ^3He in 2009 [16], and the results showed that the gamma absolute rejection ratio for neutrons, GARRn value met the requirement of ($0.9 < \text{GARRn} < 1.1$) at all the exposure rates up to 100 mR/hr, with an advantage that the boron-lined tubes can be operated at a lower voltage than the ^3He tubes. In 2013, Walker described a specified computational methodology for designing spectrally-matched plug-in replacements for a baseline ^3He detector. The alternative designs used contain BF_3 gas tubes, and a ^{10}B lining detector tube with forty-seven neutron energy groups, ranging from 0.1 eV to 17.3 MeV. The two designs demonstrated equivalent results to the ^3He detector by matching the adjoint function and reaction rate [17].

Lintereur, in 2013 [18], explored He-3 free multiplicity counter configurations including simulations, measurements, and theoretical corrections. A thermal neutron detector was developed by $^6\text{LiF}/\text{ZnS}$ sheet layered with a plastic light guide. It was found that the gamma ray sensitivity of $^6\text{LiF}/\text{ZnS}$ is higher than the gamma ray sensitivity of He-3.

In 2014, Okowita [19], tested a lithium fluoride zinc sulphide ($^6\text{LiF}:\text{ZnS}(\text{Ag})$) detector as an alternative to ^3He detector by comparing the experimental results of absolute neutron detection efficiency, gamma absolute rejection ratio, moderation response, and changing temperature, for both Li-6 and He-3 detectors. Also an MCNP simulation was conducted in association with experimental results to ensure its detection efficiency. Calculated results for absolute detection efficiency and gamma absolute rejection ratio for neutrons showed that Li-6 Aspect detector is a viable alternate to He-3 detector in RPMs.

Chapter 2: Theory and Methods

2.1 Neutron Source

The neutron generator at the Department of Nuclear Engineering – University of Sharjah was used as a thermal-neutrons source. It is an axial radio frequency induction (RFI) plasma neutron generator utilizing Deuterium-Deuterium (D-D) fusion reactions to generate 2.45 MeV neutrons with a maximum neutron yield of 4×10^9 neutrons/s and manufactured by Adelphi Technology, Inc. [20]. The generator is moderated by high-density polyethylene (HDPE) that thermalizes fast neutrons and shields thermal neutrons by borated polyethylene (BPE) surrounding the HDPE. Layers of (aluminum and lead) surrounding the HDPE to shield gamma rays and to reduce the dosage to public access levels. The dimensions of the generator with HDPE shielding are approximately (184 cm × 103 cm × 107 cm). Three ports are available for placing materials for applications like Neutron Activation Analysis (NAA), or for controlling the neutron flux distribution by inserting HDPE discs with varying moderator thickness in the ports. One of the ports can be used for fast neutron emission by completely removing the port moderator and plug.



Figure 2: Moderated & Shielded DD109.4 Neutrons-Generator at University of Sharjah [21]

2.2 Detectors

Three detectors were used in this research; NaI detector, He-3 detector and BF3 detector.

2.2.1 NaI Detector

NaI(Tl) detector is an inorganic scintillator detector and considered as the most commonly used scintillator for gamma ray detection. The NaI crystal is commonly doped with Thallium as an activator. The relatively high density ($3.67 \times 10^3 \text{ kg/m}^3$) and high atomic number ($Z=53$) make NaI a very efficient gamma-ray detector of considerably low cost in comparison to semiconductor gamma-ray detectors. In addition, its light-conversion efficiency is the highest among all inorganic scintillators with fast response decay-time of "0.23 μs " [5]. When gamma rays (ionizing-radiation) pass through the crystal, excitation occurs as electrons are raised to the conduction band of the crystal material and holes are created in the valence band. As a result of de-excitation, photons (light) are emitted (scintillation).

The activator (thallium atoms) increases the amount of emitted light by adding more excited energy-states and a photocathode is used to convert the incident photons into low-energy electrons. The electrons accelerate by the very high voltage at the photomultiplier tube (PMT) and multiplied from a few hundreds to $\sim 10^7$ - 10^{10} through the electron multiplier until being detected as a signal at the measuring device. Figure 3 illustrates the block diagram of the detection system [1].

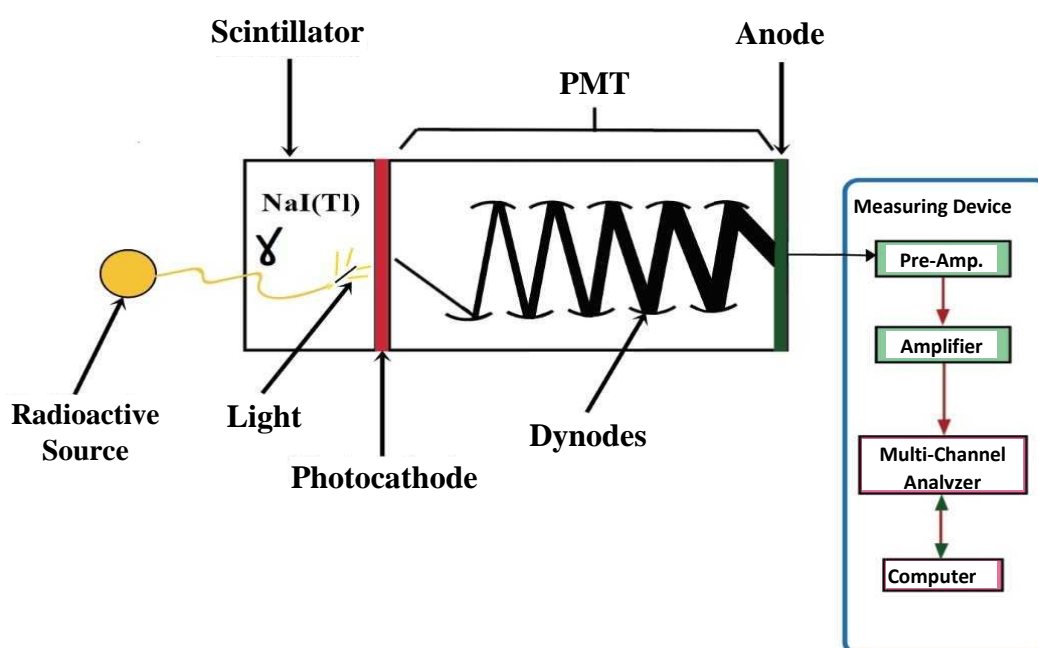


Figure 3: Block Diagram of the Detection System of NaI Detector

There are many possible interactions that play a role in how the energy spectrum appears. Figure 4 shows a typical spectrum resulting from the possible gamma interactions from Co-60, such as photoelectric effect, Compton scattering, pair production, annihilation photons, single and double escape of annihilation photons. The output voltage is proportional to the energy of gamma rays deposited in the detector [1].

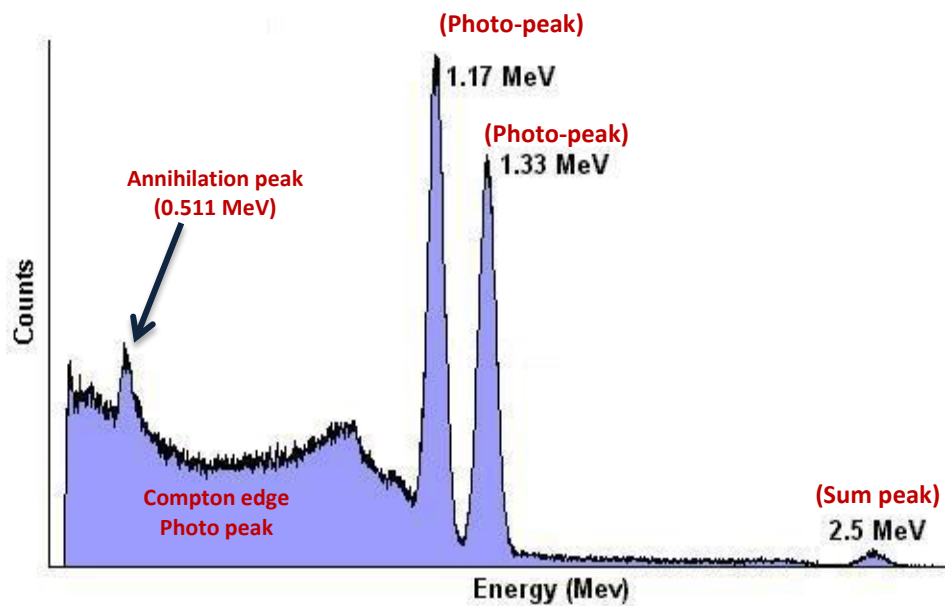


Figure 4: Pulse Height Spectrum from a NaI(Tl) Scintillator for Gamma Rays Emitted by ^{60}Co

2.2.2 Description of Boron-Lined NaI Detector

The proposed detector was prepared by covering the NaI(Tl) scintillator detector with a layer of natural boron of 0.2 cm thickness (which is more than few mean free paths of thermal neutrons $\lambda_{\text{(natural boron)}} \sim 0.01 \text{ cm}$). Natural boron is composed of 80.1% ^{11}B and 19.9% ^{10}B . Figure 5 illustrates that the boron layer acts as a converting medium that captures the neutrons incident from the surrounding and releases α -particles and 6% stable lithium nuclei and 94% excited lithium nuclei which consequently decay emitting gamma rays with energy 0.478 MeV that can be detected inside the NaI effective volume [1].

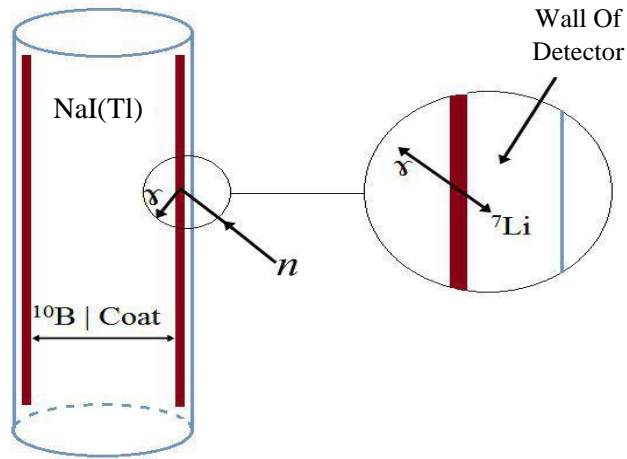
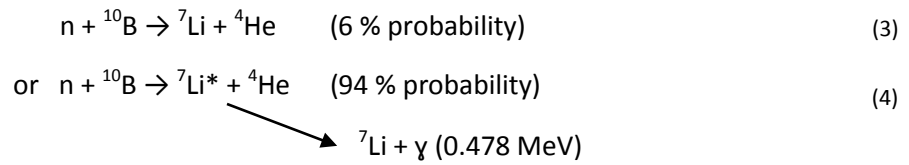


Figure 5: Boron Layer Covering NaI Detector

2.2.3 BF₃ Detectors

Boron trifluoride detector is a proportional gas-filled detector used for neutrons detection. The boron trifluoride gas undergoes (n, α) reaction with the incident thermal neutrons from the surrounding, the thermal neutron cross section of ^{10}B is 3840 barn. The $^{10}\text{BF}_3$ gas acts both as a sensitive and ionizing medium and is, therefore, usually enriched to more than 90% ^{10}B in order to enhance the efficiency of detection. When a thermal neutron enters the detector, the probability of nuclear reaction is high and may result in an event as in Figure 6.

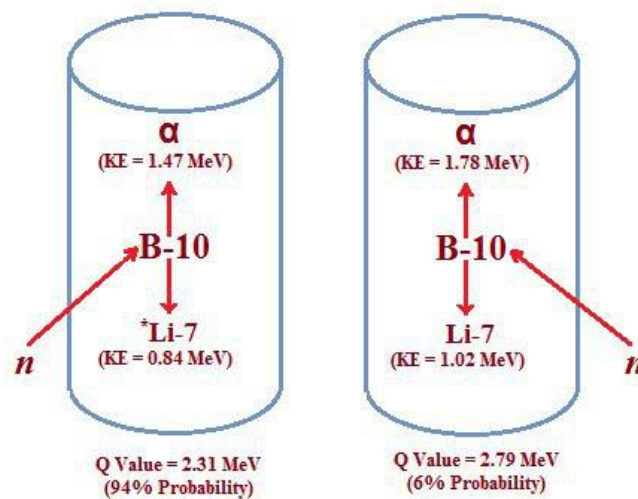


Figure 6: Interaction of Incident Neutrons with BF₃ Gas

The ionized lithium and helium cause ionization of BF₃ gas by electrostatic interactions while electrons under high voltage are accelerated and cause charge multiplication. The collected charges at the anode are proportional to the initial ionization. The energy deposited in the effective volume of the detector controls the shape of the spectrum generated. Figure 7 shows a typical pulse height spectrum for BF₃ detector as a screen shot from MAESTRO ORTEC software, which illustrates the peak of interest at energy 2.31 MeV.

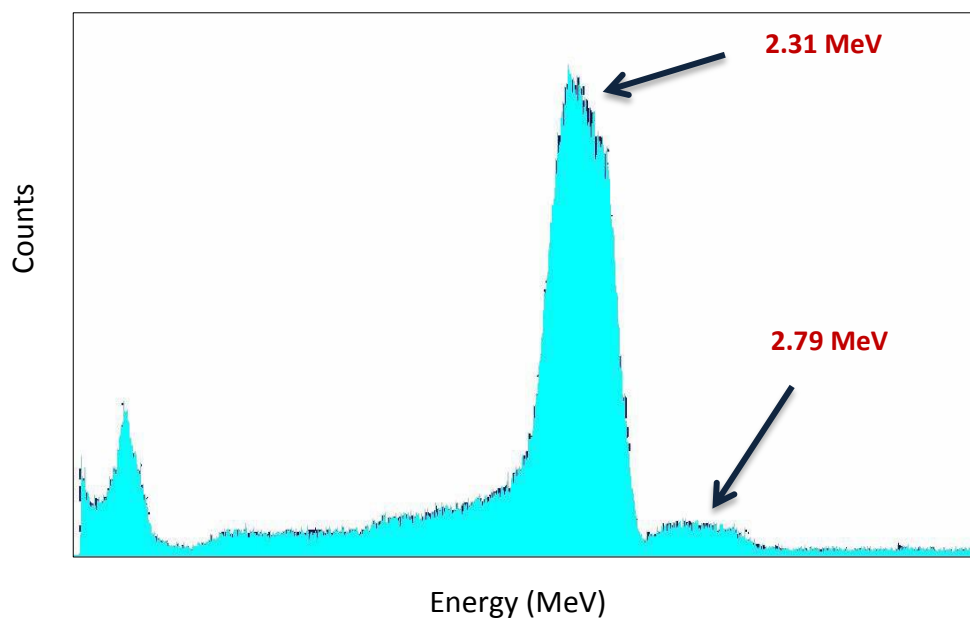


Figure 7: Typical Pulse Height Spectrum from BF₃ Detector

2.2.4 He-3 Detectors

Helium-3 detector is a gas proportional counter used for thermal neutrons detection. Typically, it has a cylindrical shape with different range of lengths. Casing is stainless steel and the anode is a wire along the axis of the cylinder. The detection is based on the following reaction.



The triton and proton ionize the He-3 gas atoms releasing electrons which migrate to the anode forming the electric pulse. If the proton and triton deposit all their energy in the ionizing gas inside the detector, the peak displays at 764 KeV. Otherwise, a plateau shows in the energy distribution spectrum at 191 KeV and 573 KeV due to the wall effect from the triton and the proton respectively as shown in Figure 8.

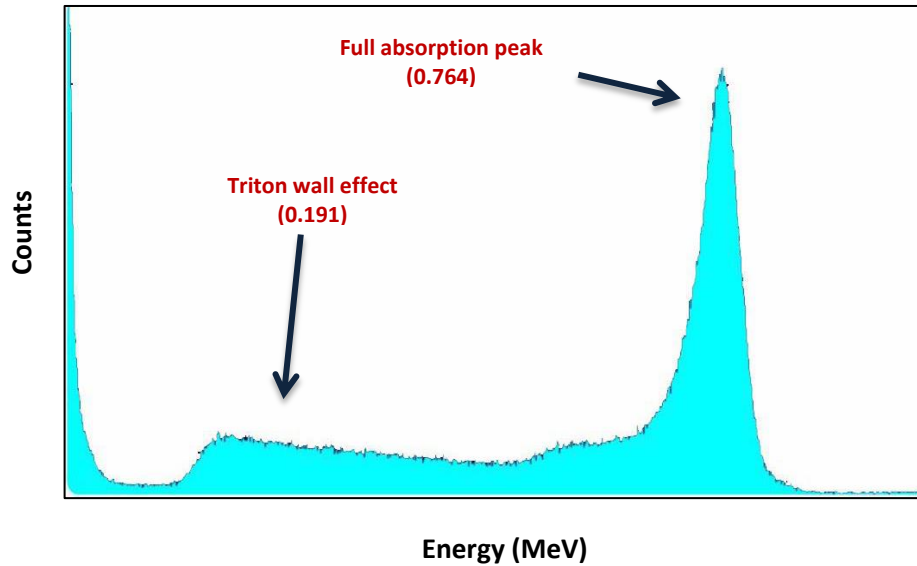


Figure 8: Typical Pulse Height Spectrum for He-3 Detector

2.3 Simulation

Testing the performance of radiation detection systems usually requires frequent changes in the design and possibly building several demos which may be considered practically difficult and complicated. Numerical simulation provides a valuable and reliable alternative where designs can be modeled and optimized more efficiently than experiments. Even though, the simulation methodology must be validated versus experimental data. The commonly used simulation method for radiation problems is the Los Alamos National Laboratory Monte Carlo N-Particle transport code [22]. MCNP can be used to model radiation transport for neutrons, photons, and/or electrons, depends on the simulated random path from one interaction to the next. The probability and outcome of each interaction is obtained from probability distributions, which represent the laws of physics for the transported neutron and sampled randomly, according to material cross-section which are built into the code.

MCNP codes use random number generators to produce random variates from a uniform distribution on the interval $[0, 1]$. These random variates are then used in subsequent sampling from probability distributions to simulate the physical behavior of particles during the transport process [23]. MCNP randomly samples particle transport to determine what, if any, events will occur based on physics (rules) and transport data (probabilities). Figure 9 illustrates an example of the history of an incident neutron on a piece of fissionable block. Event 1 is a collision releasing a photon and a scattered neutron, the photon undergoes a capture at event 2 while the direction of the scattered neutron is randomly selected from a physical scattering distribution and undergoes a fission reaction at event 3, resulting in death of the neutron and the production of two new neutrons and a photon. The photon from

fission is retrieved and allowed to undergo a collision at event 4, and leaks out at event 5. One of the fission neutrons is retrieved for analysis and via random sampling is determined to escape out of the block at event 6, while the second fission neutron is captured at event 7 [24]. All seven events represent one neutron history. The more the histories, the more accurate distributions represent reality. MCNP helps the user to adapt the modeling with a variety of options including different radiation sources, geometries, and cross sections. It also enables the calculation of different kinds of outputs (tallies) such as the pulse height, volume flux, and surface flux in addition to tally multipliers which enable to calculate the dose rate.

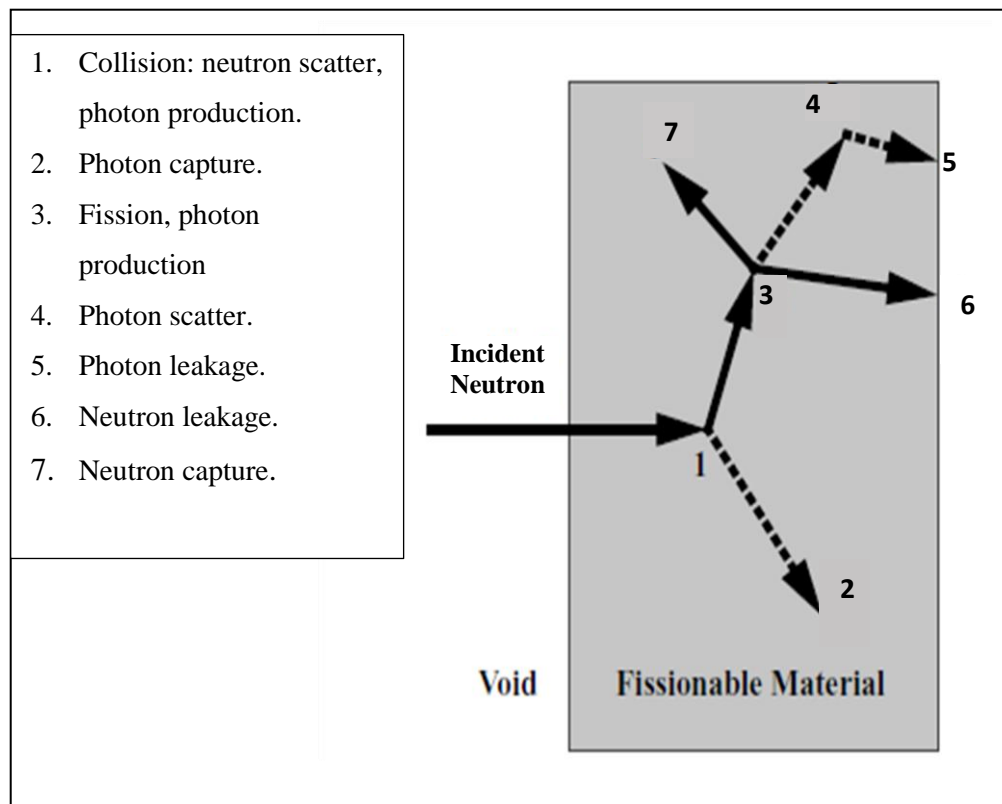


Figure 9: Particle History Example for Neutron Incident on Fissionable Block [24]

MCNP version 6.1 [25] was used to model the generator and the detection setup. A model of the generator and detectors alignment is shown in Figure 10. In order to create an MCNP input file, certain information was required including geometry specifications (cells and surfaces), description of materials, location/characteristics of the source, tallies desired, and any variance reduction techniques. The VISual EDitor (VISED) of MCNP was essential to draw the geometry and to edit the specifications. Surfaces were defined using RPP and RCC macro bodies for parallelogram and cylinders respectively, and based on the dimensions taken from manufacturer's provided drawings for the generator and detectors. Digimizer Images Analysis Software was used to take accurate dimensions of the components of the generator from the manufacturer's provided drawings [26].

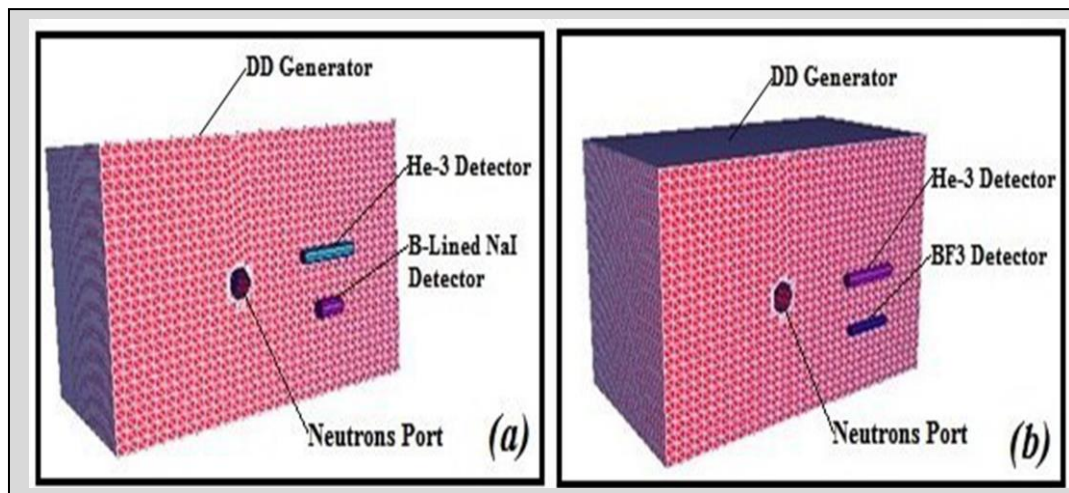


Figure 10: DD Neutron Generator Setup with a) He-3 and Boron-Lined NaI Detectors. b) He-3 and BF3 Detectors.

2.3.1 Surface Cards

Figure 11 illustrates a two-dimensional XY cross section of the generator with some of surfaces written on each part as a screen shot from Vised Software. Surfaces 1–3 represent the outer shielding of the generator (1.3 cm lead with 0.3 cm aluminum both sides all around the lead). While surfaces 4, 5 represent the outer and inner surfaces of BPE shielding. Surfaces 6–8 represent the inner shielding of the generator (1.3 cm lead with 0.3 cm aluminum both sides all around the lead). Surface 9 represents the HDPE shielding (49.21 cm × 43.82 cm × 44.91 cm) filling all around the cylinder of generator. Surface 10 represents the D-D 109.4 generator cylinder. Surfaces 13, 15 represent the opened front port and HDPE moderator disc respectively. Surfaces 14 and 16 represent the closed back port and BPE sample plug respectively. Surfaces 17 and 18 represent the HDPE all around the generator. Surfaces 558–561 represent the source.

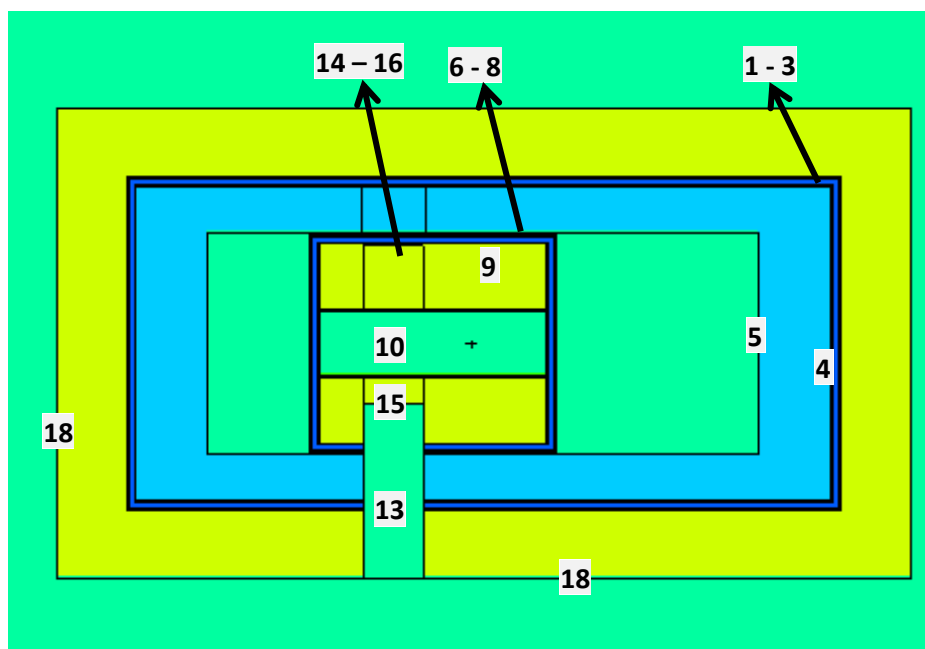


Figure 11: XY Section of MCNP Generator Model Surfaces

2.3.2 Cell Cards

Figure 12 shows the MCNP model of the neutrons generator and detectors with cells alignments at ($x=15$, $y=-20$, $z=0$). Cells 20, 30 and 40 were filled with aluminum, lead and aluminum respectively and represent the main outer shielding layer of generator while cell 50 represents the Borated-Polyethylene layer. Cell 60 represents the space around the inner shielding and is filled with air. Cells 70, 80 and 90 were filled with aluminum, lead and aluminum respectively, and represent the main inner shielding layer of the generator. Cells 100 and 108 filled with HDPE and represent the shielding of the cylinder and outer shielding layers, respectively. Cell 102 represents the main generator cylinder. Cells 119 and 120 represent the casing and tube of He-3 detector, while cells 115–117 represent B-layer, aluminum, and tube of NaI detector respectively.

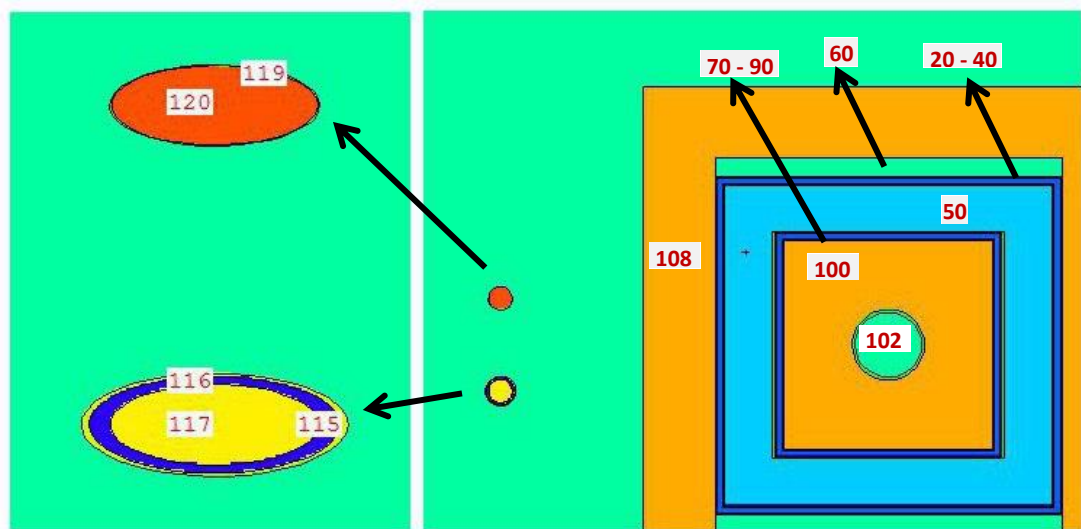


Figure 12: YZ Section of MCNP Alignment Cells

2.3.3 Materials

Material specification in MCNP follows the format (*Mn ZAID₁ fraction₁ ZAID₂ fraction₂*). The *n* represents the material number; ZAID corresponds to either the full ZZZAAA or partial ZZZAAA element or nuclear identifier (ZZZ is the atomic number, AAA is the atomic mass number) and *fraction* corresponding to the atomic fraction (or weight fraction if entered as a negative number) [7]. Table 2 shows the partial ZAID used and the corresponding weight fraction for all materials used in this model. All materials were retrieved from Compendium of Material Composition Data for Radiation Transport Modeling by PNNL [27]. Below is a part of input file illustrating the materials used.

```

c -----Natural Boron-----
m7      5010. -0.199  5011. -0.801          $ B-10, B-11
c ----- Sodium Iodide -----
m8      11023. -0.153373  53127. -0.846627    $ Na, I
c ----- HDPE(Polyethylene non borated) PNNL page 239
m9      1001.          -0.143716             $ Hydrogen
        6000.          -0.856284             $ Carbon
c ----- Copper -----
m17     29000.          -1

```

Table 2: Materials Specification Used in MCNP

Material	Material #	ZAID	fraction
Aluminum	m1	13027	-1
Lead	m2	82000	-1
BPE	m3	6000	-0.813466
		1001	-0.136534
		5010	-0.0092155
		5011	-0.0407845
Air	m4	6000	-0.000124
		7014	-0.755268
		18000	-0.012827
		8016	-0.231781
Stainless Steel	m5	6000	-0.00041
		14000	-0.00507
		15031	-0.00023
		16000	-0.00015
		24000	-0.17
		25055	-0.01014
		26000	-0.669
		28000	-0.12
Ground	m6	42000	-0.025
		1001	-0.00453
		8016	-0.5126
		11023	-0.01527
		13027	-0.03555
		14000	-0.36036
		20000	-0.05791
		26000	-0.01378
Natural Boron	m7 (setup 1)	5010	0.199
		5011	0.801
BF3	m7 (setup 2)	5010	-0.031728
		5011	-0.127711
		9019	-0.840561
Sodium Iodide	m8	11023	-0.153373
		53127	-0.846627
HDPE	m9	1001	-0.143716
		6000	-0.856284
He-3	m10	2003	-1
Copper	m17	29000	-1

2.3.4 Tallies

Estimating the neutron response of each detector requires information about the kind of interaction inside the detector. For boron-lined NaI, a flux tally (F4) was used to estimate the neutron flux in the boron layer (cell 115) and tally E4 for the energy binning of neutrons (classify the number of neutrons equally according to energy) into 1000 bins from 0 eV to 2.45 MeV. Pulse height (F8) tally was used to obtain the resulting gamma spectrum in the NaI detector (cell 117); energy binning E8 was used to divide the range from 0 to 10 MeV into 1024 bins. For He-3 and BF3 detectors, the flux tally (F4) was used and modified with the tally-multiplier (Fm card) to count the number of (n,p) and (n, α) reactions respectively by multiplying the number of neutrons in each detector by certain data library value according to the specific kind of interaction of interest, in our work it is the total absorption cross section of thermal neutrons. The simulation was performed for 2 billion histories to reach to a relative error (RE) less than 10% in each of the energy bins of interest according to the equation $RE \sim 1/(\sqrt{N})$, Where N is the total number of histories. Below is a part of an input file that illustrates the tallies used for the three detectors.

```
c ##### TALLY#####
c ----- NaI detector -----
f4:n 115          $ neutrons flux in B layer
e4: 0 1000i 2.45  $ neutron energy binning in B layer
f8:p 117          $ Pulse height in NaI detector
e8: 0 1024i 10    $ photon energy binning in NaI
c ----- He-3 Detector -----
f14:n 120         $ neutrons flux for He-3 detector
fm14 (-1 10 103)  $ tally multiplier for (n, p) reaction
c -----BF3 Detector -----
c f4:n 117        $ neutrons flux in BF3
c fm4 (-1 7 107)  $ tally multiplier for (n, $\alpha$ ) reaction
```


2.3.5 Simulation Variables

a. Change of neutrons flux (by changing HDPE port moderator thickness)

A set of MCNP input files were prepared in order to check the effect of changing the neutron flux (by changing the thickness of HDPE port moderator) on the response of each detector. Boron-lined NaI and He-3 detectors were symmetrically aligned to the neutrons source; the center of the effective volume of each detector was placed at 30 cm from the edge of the front port of the generator and at 30 cm apart from the front face. He-3 was placed 10 cm above the horizontal plane of neutrons source while B-lined NaI or BF₃ was placed 10 cm below the horizontal plane of neutrons source. To change the thickness of HDPE moderator, the length of the cylinder (surface 15) was adjusted as the desired thickness to simulate the actual thicknesses of HDPE discs in laboratory. Below is a part of one of the input files illustrating the surface card of HDPE port moderator with thickness (1.28 cm).

```
C ----- Surface -----
15 rcc -16.8 -7.601 0 0 -1.28 0 6.4      $ HDPE front port moderator
```

b. Change of neutron flux (by changing the detectors distance from the neutrons port)

Three MCNP input files were prepared to investigate the effect of changing the neutrons flux (by changing the distance of detectors from the neutrons port) on the response of each detector. B-lined NaI and He-3 detectors were symmetrically aligned to the front port of the generator; while the center of the effective volume of each detector was placed 30 cm, 40 cm and 50 cm to the right edge of the front port of the generator. Same set of input files at same distances were prepared for comparison between He-3 and BF₃. Thickness of HDPE moderator was fixed at 5.06 cm inside the generator port for the 3 simulations.

2.4 Measurements

Experiments were carried out at the central laboratories of Sharjah University, Department of Nuclear Engineering. The DD neutron generator was used as the neutron source. Some of the detectors' specifications are listed in Table 3. Each experimental measurement was run for approximately five minutes to accumulate enough counts in the peaks of interest and decrease the relative error to less than 5%.

2.4.1 Detectors Specifications

Some specifications of the detectors used in this work are presented in Table 3.

Table 3: Some Specifications of NaI, He-3 and BF3 Detectors

	NaI	He-3	BF3
Manufacturer	ScintiTech	LND	LND
Diameter (cm)	5.08	5.08	3.91
Effective Diameter (cm)	5.04	4.98	3.81
Length (cm)	12.7	39.22	58.5
Effective Length (cm)	12.7	30.99	25.4
Casing (cm)	Aluminum 0.5	Stainless Steel 0.05	Stainless Steel 0.05
Other	Wrapped with 0.2 cm of natural boron	Pressure: 2063 Torr	Pressure: 650 Torr
Voltage	670 V	1022 V	1909 V

2.4.2 Experiments

The experimental arrangement was the same as in the MCNP simulation while additional measurements were performed to validate the effect of changing the neutron flux (by changing the generator power) on the response of each of the three detectors. Figure 13, shows the front port of generator and HDPE discs with various thicknesses. Three series of experiments were performed to analyze the response of the detectors to perturb the neutron flux. In each experiment two detectors were placed symmetrically with respect to the neutrons source. These experiments were:

1. HDPE discs of varying thickness were inserted in the neutron port, while the position of the detectors and the neutrons generator power were fixed.
2. The position of the detectors was varied, while HDPE moderator thickness and neutrons generator power were fixed.
3. The neutrons generator power was varied, while HDPE moderator thickness and the detectors position were fixed.

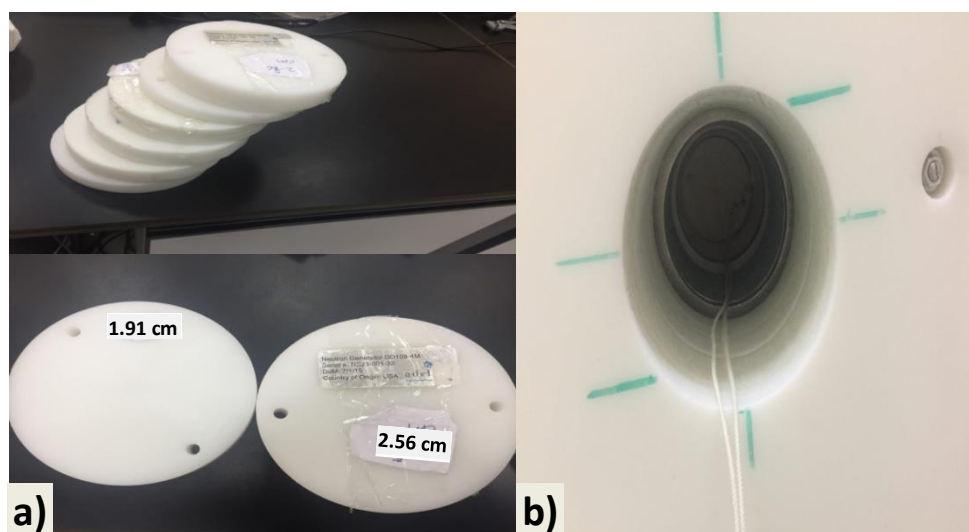


Figure 13: a) HDPE Port Moderator Discs, b) Generator Front Port.

2.4.3 Experimental Setup

Two setups were adjusted as explained earlier and are shown in Figure 14 and Figure 15.

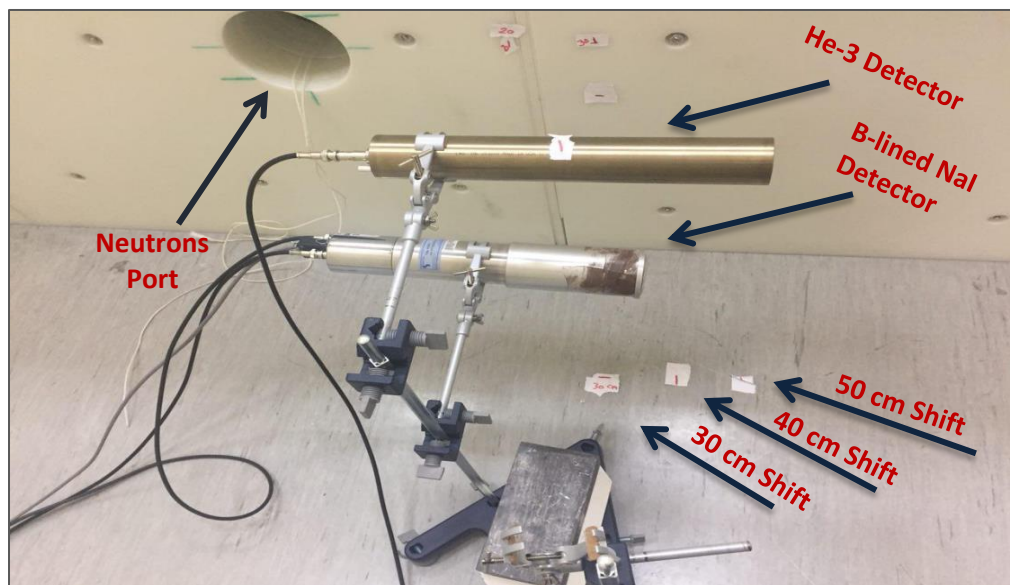


Figure 14: He-3 and B-Lined NaI Detectors at 30 cm from the Neutrons Port

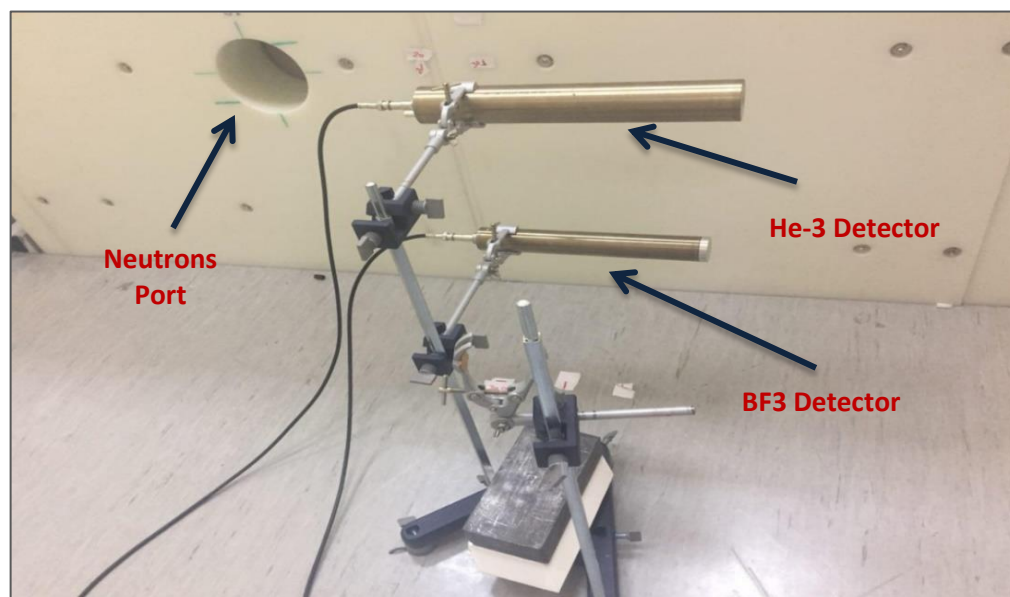


Figure 15: He-3 and BF3 Detectors at 50 cm from the Neutrons Port

Each detector was connected to high voltage power supply and the output signal connected to a preamplifier, amplifier, and a multi-channel analyzer (MCA) as shown in the block diagram in Figure 16. The MCA was set to 2048 channels and the spectrum from each detector was collected and analyzed using the Ortec MAESTRO software.

The following sequence was followed for each detector at each setup:

- Setting the voltage and coarse gain then adjusting the fine gain to make sure that the desired peak is located at the specific location.
- Running the generator.
- Fixing the measurement time ~ (5 minutes)
- Obtaining the spectrum from each detector.

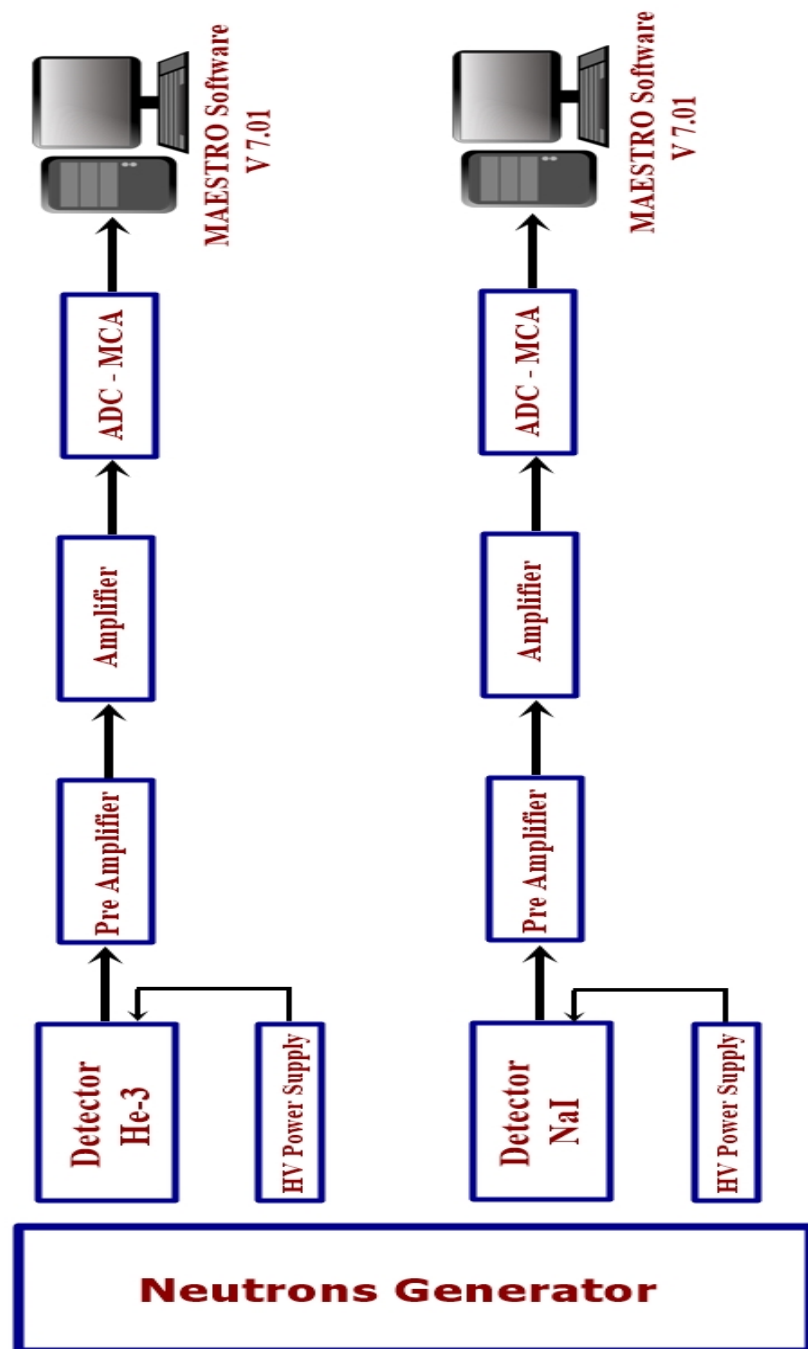


Figure 16: Block Diagram of the Detectors and Neutron Generator

2.5 Net Counts and Error propagation

2.5.1 Sigma for MCNP calculations

Error bars were added to the plots where applicable. The standard deviation was simply calculated for BF3 and He-3 detectors from relative error of MCNP tally results for each bin.

The net counts (X) in the peak of B-NaI detector were calculated by subtracting the range from the summation of counts of peak of interest which presented by the following equation:

$$X = \sum_{i=N}^M C_i - \left[\left(\frac{C_N + C_M}{2} \right) (M - N + 1) \right] \quad (6)$$

Where:

$\sum_{i=N}^M C_i$: total counts in the peak

N, M : starting and ending channel of peak respectively

C_N, C_M : Counts in starting and ending channel of peak respectively

To simplify the equation, we can represent $\sum_{i=N}^M C_i$ as S, $\frac{M-N+1}{2}$ as constant K

$$X = S - K * (C_N + C_M) \quad (7)$$

$$S = \sum_{i=N}^M C_i = C_N + C_{N+1} + C_{N+2} + \dots + C_M \quad (8)$$

The standard deviation, S and σ_N , for the counts were calculated using the Taylor series expansion through the following derivation.

$$\sigma_s^2 = \left(\frac{\partial s}{\partial C_N} \right)^2 \sigma_{C_N}^2 + \dots + \left(\frac{\partial s}{\partial C_M} \right)^2 \sigma_{C_M}^2 \quad (9)$$

$$= (1)^2 \sigma_{C_N}^2 + \dots + (1)^2 \sigma_{C_M}^2 \quad (10)$$

$$\sigma_s = \sqrt{\sigma_s^2} \quad (11)$$

$$\sigma_X^2 = \left(\frac{\partial X}{\partial S} \right)^2 \sigma_s^2 + \left(\frac{\partial X}{\partial C_N} \right)^2 \sigma_{C_N}^2 + \left(\frac{\partial X}{\partial C_M} \right)^2 \sigma_{C_M}^2 \quad (12)$$

$$= (1)^2 \sigma_s^2 + k^2 \sigma_{C_N}^2 + k^2 \sigma_{C_M}^2 \quad (13)$$

$$= \sigma_s^2 + k^2(\sigma_{C_N}^2 + \sigma_{C_M}^2) \quad (14)$$

$$\sigma_X = \sqrt{\sigma_s^2 + k^2(\sigma_{C_N}^2 + \sigma_{C_M}^2)} \quad (15)$$

And

$$\sigma_s = \sqrt{\sigma_{C_N}^2 + \sigma_{C_{N+1}}^2 + \dots + \sigma_{C_M}^2} \quad (16)$$

2.5.2 Sigma for experiments calculations

$$\text{Net counts rate per channel} = \frac{X}{\text{live time} \times \text{number of channel}} \quad (17)$$

Where x: is the net count in the peak from MAESTRO software according to the equation:

$$X = \sum_{i=N}^M C_i - \sum_{i=N}^M B_i \quad (18)$$

Where

$$\sum_{i=N}^M C_i : \text{total counts in the peak.} \quad (19)$$

$$\sum_{i=N}^M B_i : \text{total background in the peak.} \quad (20)$$

N, M: starting and ending channel of peak respectively.

C_N, C_M : counts in starting and ending channel of peak respectively.

$$\text{For simplicity let's } S = \sum_{i=N}^M C_i \quad \text{and} \quad D = \sum_{i=N}^M B_i \quad (21)$$

$$(\text{Constant}) K = \frac{1}{\text{live time} \times \text{number of channel}} \quad (22)$$

$$X = (S - D) \quad (23)$$

Where

$$\sigma_X^2 = \left(\frac{\partial X}{\partial S}\right)^2 \sigma_S^2 + \left(\frac{\partial X}{\partial D}\right)^2 \sigma_D^2 \quad (24)$$

$$\sigma_X^2 = \sigma_S^2 + \sigma_D^2 \quad (25)$$

$$\sigma_X = \sqrt{\sigma_S^2 + \sigma_D^2} \quad (26)$$

Where $\sigma_s = \sqrt{\sigma_s^2}$ and $\sigma_D = \sqrt{\sigma_D^2}$ similar to equations (9-11)

$$\sigma \text{ Net counts rate per channel} = \frac{\sigma_X}{\text{live time} \times \text{number of channel}} \quad (27)$$

Chapter 3: Results and Discussions

3.1 Simulation Results

After running MCNP input files, the output files were generated and the tally results were extracted. The results were further transferred to a spreadsheet for analysis and plotting. Simulation results can be found in Appendix B. All simulation results from MCNP are in counts per source particle (CPSP). The NaI detector counts were adjusted as per Table 4 to account for photons losses in the crystal and photocathode, as these losses are not accounted for in the MCNP simulations. Optical efficiency of the crystal (K) is the efficiency with which the crystal transmits light. A typical crystal might have an optical efficiency, k , of 0.5 - in other words 50% of the light produced reaches the photocathode which might have a quantum efficiency of 0.2. Quantum efficiency of photocathode (I) is the efficiency with which the photocathode converts light photons to electrons [28].

Table 4: Adjustments for NaI Detector Response [13].

Adjustment	Value (%)
(k): Optical efficiency of crystal	$\sim 50^*$
(I): Quantum efficiency of photocathode	~ 20

*Slightly decreased to account for tall detectors

3.1.1 Effect of Adding Boron Layer to NaI Detector

To investigate the effect of the boron layer on the NaI detector, two simulations were performed; one with the boron layer and the other without the boron layer around the NaI detector at the same neutron flux conditions. The HDPE port moderator thickness was fixed at 1.28 cm and the distance from the generator to the right edge of the front port was 30 cm. The He-3 detector was modeled simultaneously with the NaI detector. The F8 Tally was used to calculate the photon pulse height in the effective volume of NaI detector and photons were binned into 1024 energy bins in order to plot the pulse height spectrum. Figure 17 shows the results of these two simulations. The two spectra are identical and a significant increase in photon counts with boron are $\sim 21\%$ more than that without boron at energy region 0.5 MeV due to the γ -rays emitting from $^{10}\text{B}(n,\alpha)^7\text{Li}$ reaction. Photon peak in absence of boron layer is due to the boron in borated polyethelene layer in the generator. The peak at 0.511 MeV is the annihilation peak. All of the detailed results can be found in Table 9, Appendix B.

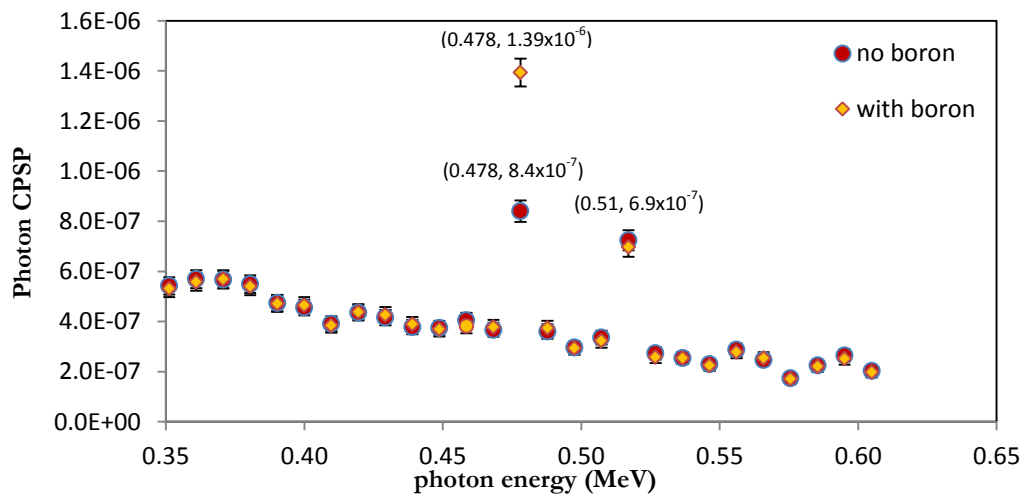


Figure 17: Simulated Pulse Height Spectrum of NaI Detector, with and without Boron Layer.

3.1.2 Effect of HDPE Port Moderator Thickness

a. Boron-lined NaI detector vs. He-3 detector

Table 5 lists the simulated counts per source particle for both detectors at varying thickness of HDPE moderator. It is clear that boron-lined NaI detector has higher counts than He-3 detector. Also included in Table 5 are the calculated uncertainties (sigma) in the counts as derived in equations (6-16) for NaI detector, while for He-3, the uncertainty is directly reported from MCNP.

Table 5: MCNP Simulated Counts at Different Port Moderator Thickness for NaI and He3 detectors

Moderator Thickness (cm)	B-Lined NaI Detector		He-3 detector	
	CPSP ¹	Sigma	CPSP ¹	Sigma
1.28	1.408E-08	1.0513E-09	9.482E-09	9.2926E-11
1.91	1.442E-08	1.0439E-09	9.366E-09	9.1786E-11
2.52	1.413E-08	1.0347E-09	9.100E-09	9.0996E-11
3.80	1.321E-08	1.0344E-09	8.288E-09	8.7023E-11
4.40	1.290E-08	1.0322E-09	7.867E-09	8.4963E-11
5.66	1.162E-08	1.0291E-09	6.837E-09	7.8627E-11
6.19	1.191E-08	1.0212E-09	6.490E-09	7.6577E-11
7.44	1.026E-08	1.0152E-09	5.476E-09	7.0092E-11
8.17	9.558E-09	1.0195E-09	5.148E-09	6.7950E-11
9.45	9.250E-09	1.0095E-09	4.251E-09	6.1633E-11
10.4	8.581E-09	1.0062E-09	3.722E-09	5.8071E-11
11.8	7.592E-09	1.0036E-09	2.977E-09	5.1499E-11
13.1	7.350E-09	1.0022E-09	2.517E-09	4.7065E-11

¹ Counts Per Source Particle

Figure 18, shows that counts decrease in both detectors by increasing the port moderator thickness (i.e. by decreasing the neutron flux). As the moderator thickness increases, neutrons interact more and lose more energy and maybe absorbed. Note that the neutrons emitted from the side port of the generator are already thermalized by the shielding layers due to the specific geometry of the generator and the port. Both detectors show a good sensitivity to the change in the neutron flux. This plot shows a very similar trend for both modules, and shows that the response of boron-lined NaI module is higher than that of He-3 detector used in this work (average relative efficiency about 1.9). While relative error in the energy bins from MCNP is less than 10% for both detectors, the results of NaI detector show higher sigma because of propagation of error at calculating the photon counts under 0.5 MeV peak by subtracting the range from the summation of counts of peak of interest. Statistical uncertainty is less than 9% and 2% for B-lined NaI and He-3 detectors respectively.

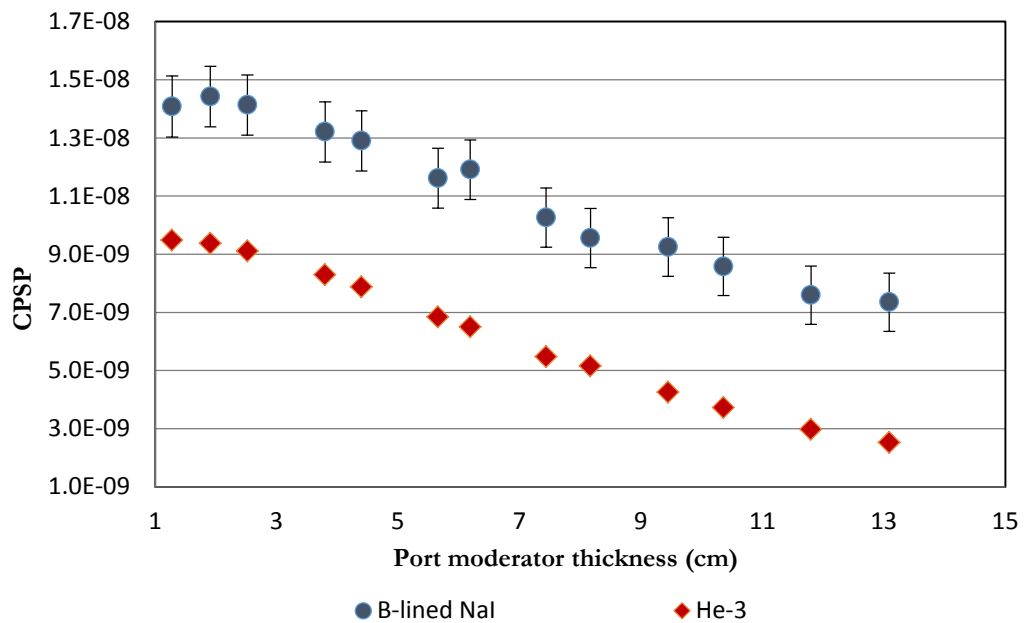


Figure 18: MCNP Simulated Net Counts in B-lined NaI and He-3 Detector at Different HDPE Moderator Thickness

b. BF3 detector vs. He-3 Detector

The estimated neutron counts for BF3 and He-3 detectors in Table 6 shows expected higher efficiency for He-3 detector. Figure 19 shows the log scale of counts per source particle in BF3 and He-3 detectors as a result of changing the HDPE port moderator thickness (i.e. changing the neutron flux). The response decreases as the port moderator thickness increases in both detectors as shown with almost the same trend, while higher response of He-3 detector than that of BF3 detector is shown. Statistical uncertainties are less than 2 %.

Table 6: MCNP Simulated Counts at Different HDPE Port Moderator Thickness for He-3 and BF3 Detectors

Moderator Thickness (cm)	He-3 Detector		BF3 Detector	
	CPSP	Sigma	CPSP	Sigma
1.28	9.675E-09	9.772E-11	9.723E-10	1.196E-11
1.91	9.424E-09	8.387E-11	9.787E-10	1.057E-11
2.52	9.177E-09	8.259E-11	9.592E-10	1.046E-11
3.80	8.450E-09	8.112E-11	8.610E-10	9.815E-12
4.40	8.019E-09	7.298E-11	8.171E-10	8.988E-12
5.66	7.029E-09	7.592E-11	7.179E-10	9.261E-12
6.25	6.437E-09	6.759E-11	6.675E-10	8.410E-12
6.90	6.004E-09	6.545E-11	6.205E-10	7.942E-12
8.20	5.061E-09	7.339E-11	5.059E-10	8.650E-12

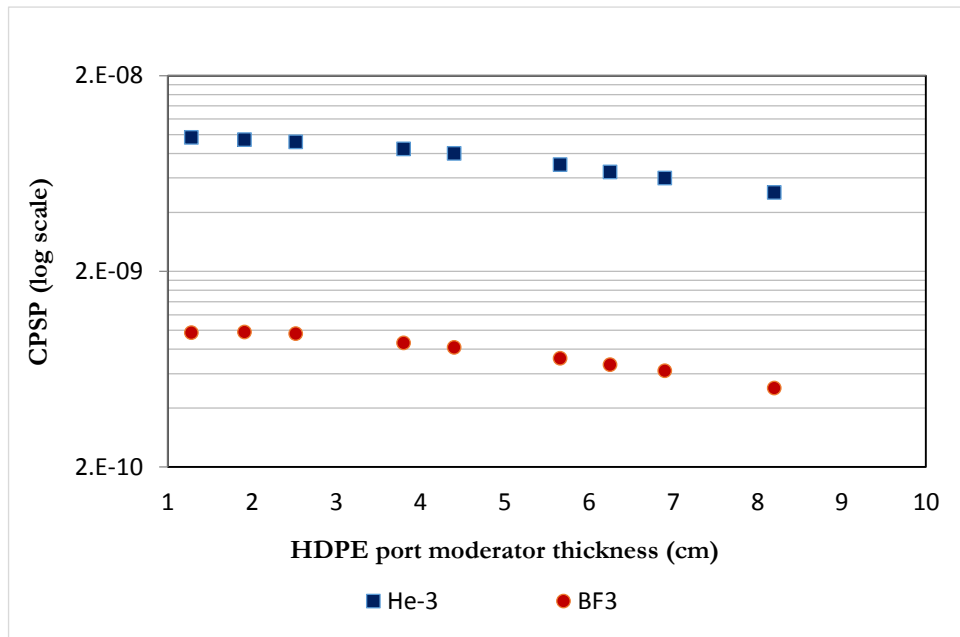


Figure 19: MCNP Simulated Net Counts in BF3 and He-3 detector at different HDPE Port Moderator Thicknesses

3.1.3 Effect of Detectors Distance from the Port

Table 7 and Table 8 show the simulated counts per source particle of B-lined NaI and He-3 detectors as a result of changing the distance from the side port of the neutron generator (i.e. changing the neutron flux); at fixed port moderator thickness.

Table 7: MCNP Simulated Counts in B-Lined NaI and He-3 Detectors at Different Distances from the Port

Distance (cm)	B-lined NaI Detector		He-3 Detector	
	CPSP	Sigma	CPSP	Sigma
30	1.209E-08	1.029E-09	7.434E-09	8.252E-11
40	1.011E-08	9.266E-10	4.919E-09	7.034E-11
50	7.764E-09	8.343E-10	3.122E-09	5.494E-11

Table 8: MCNP Simulated Counts in He-3 and BF3 Detectors at Different Distances from the Port

Distance (cm)	He-3 Detector		BF3 Detector	
	CPSP	Sigma	CPSP	Sigma
30	7.504E-09	6.379E-11	7.54488E-10	3.38057E-11
40	4.784E-09	5.119E-11	5.01182E-10	2.85952E-11
50	3.217E-09	4.214E-11	3.51731E-10	2.41161E-11

Figure 20 shows the adjusted counts per source particle in B-lined NaI and He-3 detectors at difference distances from the side port of generator. Counts per source particle (CPSP) decrease as the detector is shifted away from the neutron port in both detectors as a result of the neutron flux decrease. B-lined NaI shows a higher efficiency than He-3 detector at the three distances and the average relative efficiency ~ 2 . Good sensitivity to the change in the neutron flux is shown from both detectors.

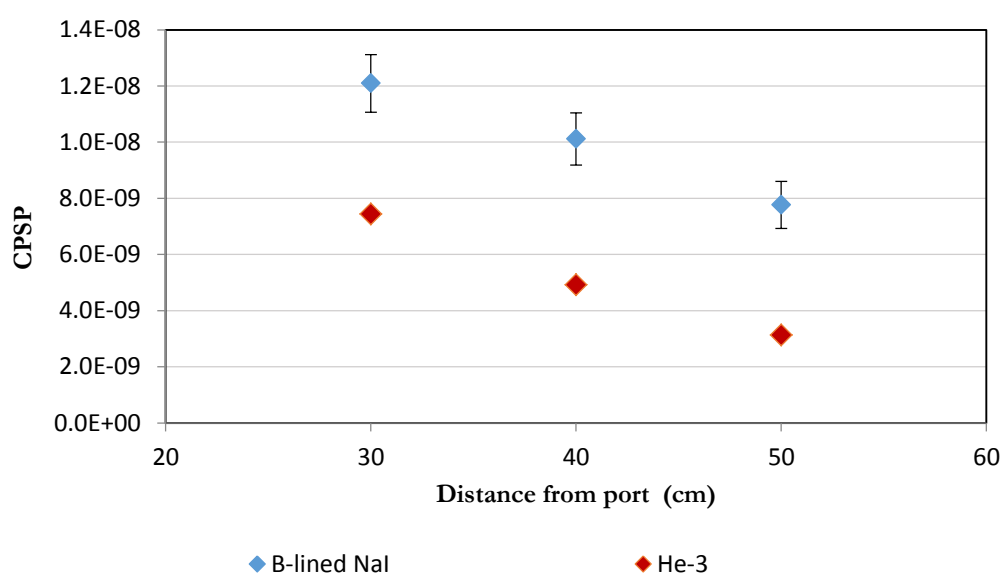


Figure 20: MCNP Detector Response of B-lined NaI, He-3 at Various Distances from the Port

Figure 21 shows the simulated neutrons count in He-3 and BF3 detectors at various distances from the neutrons port, at fixed HDPE port moderator thickness. Counts decrease as the distance increases in both detectors almost with the same trend, and as expected higher counts in He-3 detector than that of BF3 detector is shown.

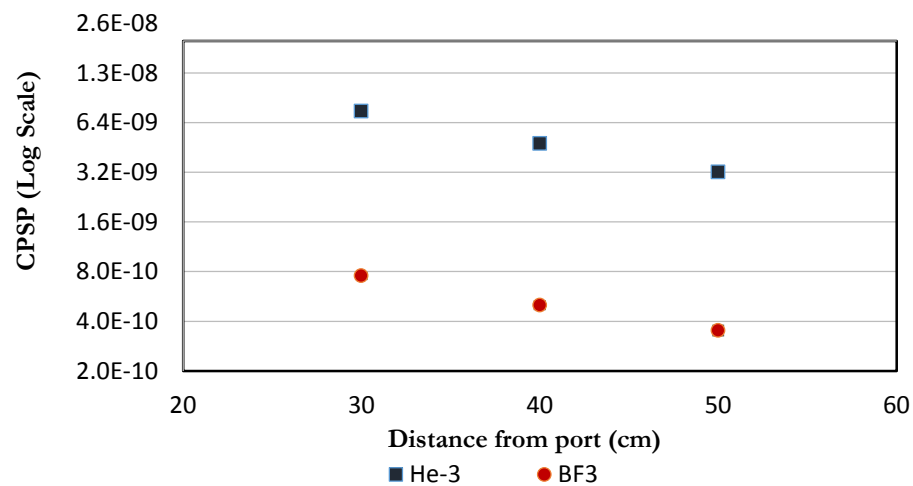


Figure 21: MCNP Detector Response of He-3, BF3 at Various Distances from the Port

3.2 Experimental Results

To validate the effect of the boron layer on the NaI detector, two experiments were performed at the same neutron generator operating conditions; one with the boron layer and the other without the boron layer around the detector. Figure 22 shows the results of these two experiments. As expected, the resolution of the NaI detector did not allow for separation of the 0.511 annihilation peak and the 0.478 peak resulting from the boron-10 (n, α) reaction. It is clear from the figure that the boron layer has a significant effect in increasing the number of counts in the 0.5 MeV region $\sim 30\%$ and a consequent effect in shifting the peak centroid below 0.511 MeV.

The counts in the 2.2 MeV region, is due to the emission of 2.223 MeV gamma rays as a result from thermal neutrons total absorption by HDPE through reaction $^1\text{H}(\text{n},\gamma)^2\text{H}$.

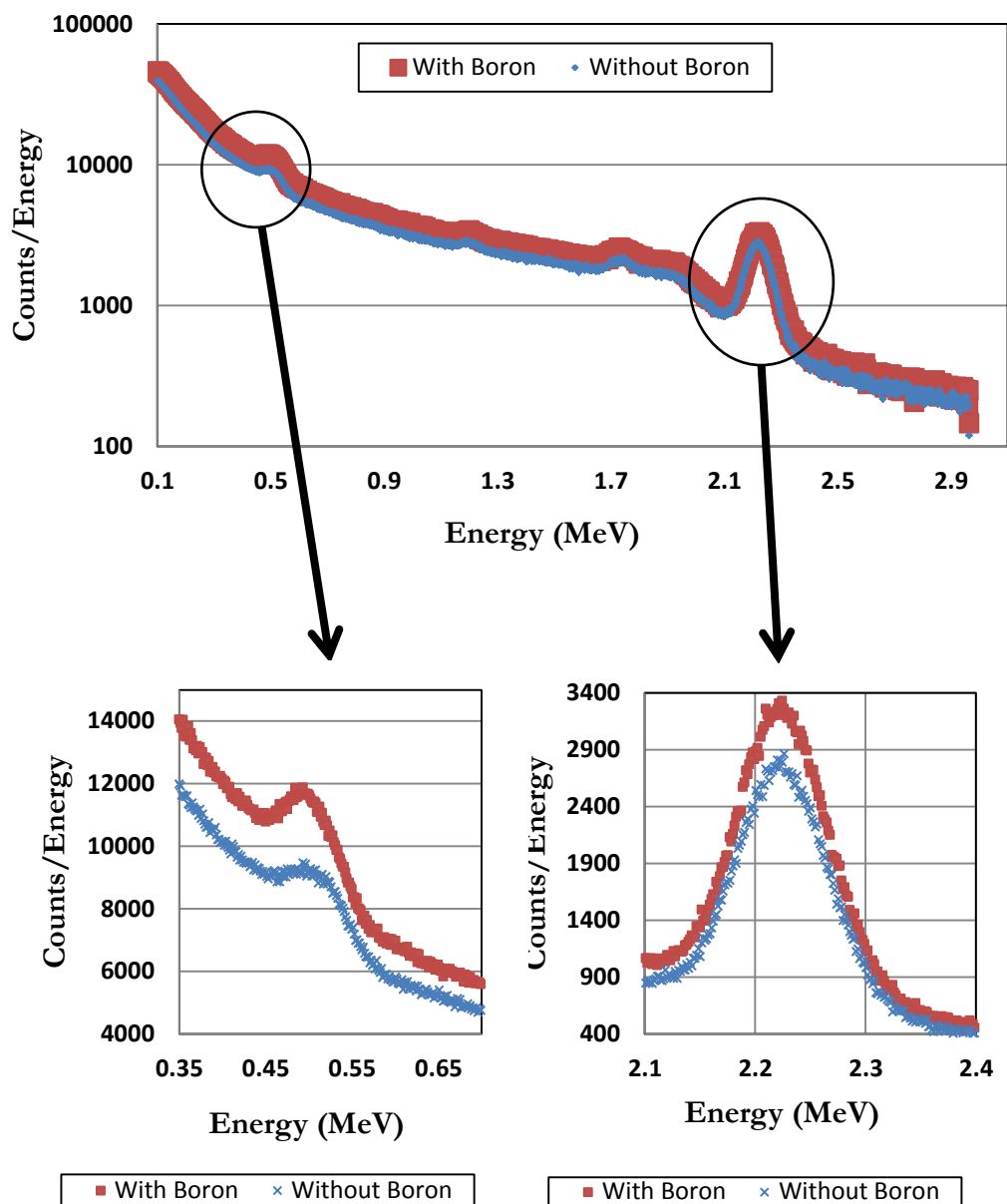


Figure 22: Gamma Ray Spectrum in NaI detector, with and without Boron Layer

Figure 23 shows the experimental net counts rate per channel (Net CPS/channel) in B-lined NaI and He-3 detectors for various HDPE port moderator thicknesses. The net counts were calculated by subtracting the continuum counts under the peaks. For the NaI spectrum the net counts were considered as that combined peak ranging from the 0.478 to the 0.511 energy. For the He-3 spectrum the counts under the 0.764 MeV peak were considered. The dead time in the detectors ranged from 20-40%; depending on the experiment performed. The live time was used in calculations to account for this dead time. It can be seen from the figure that both detectors have a good sensitivity to the changes in the neutron flux and that their response decreases with the increase in moderator thickness almost with the same trend, in addition to the higher counts in B-Lined NaI than that of He-3 detector. Detailed results can be found in Table 10, Appendix C. The standard deviation is less than 4%.

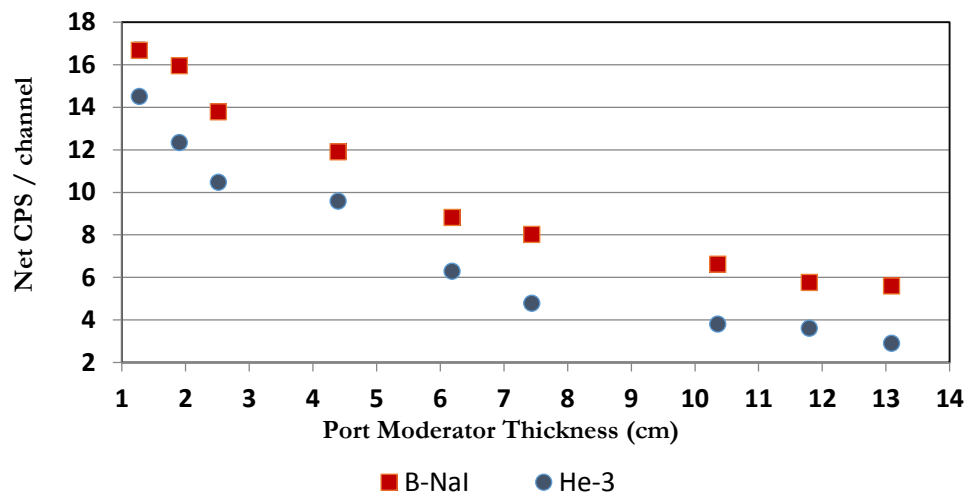


Figure 23: Experimental Net Counts in B-lined NaI and He-3 Detectors, Generator Power (2000 W).

Figure 24 shows the experimental Net CPS/channel for BF3 and He-3 detectors of various HDPE port moderator thicknesses. The net counts were calculated by subtracting the continuum counts under the peaks. For the He-3 and BF3 spectrum the counts under the 0.764 MeV peak and 2.31 MeV peak were considered respectively. Counts at thickness 1.28 cm and 1.91 cm were eliminated from the graph, because of the instability of the neutron generator during these experiments. It can be seen from the graph that He-3 detector shows higher efficiency than that of BF3 detector with average relative efficiency ~ 1.4 . Both detectors show almost the same sensitivity to the changes in the neutron flux. By comparing the Simulation and experimental results of BF3 detector, a difference by a factor of about 10 was observed. This could not be explained as the same specifications were simulated (pressure, density, active volume). Similar observation was made by researchers while comparing the detection efficiency of BF3 [29]. This discrepancy needs to be investigated further. Detailed results can be found in Table 11, Appendix C. Standard deviation is less than 4%.

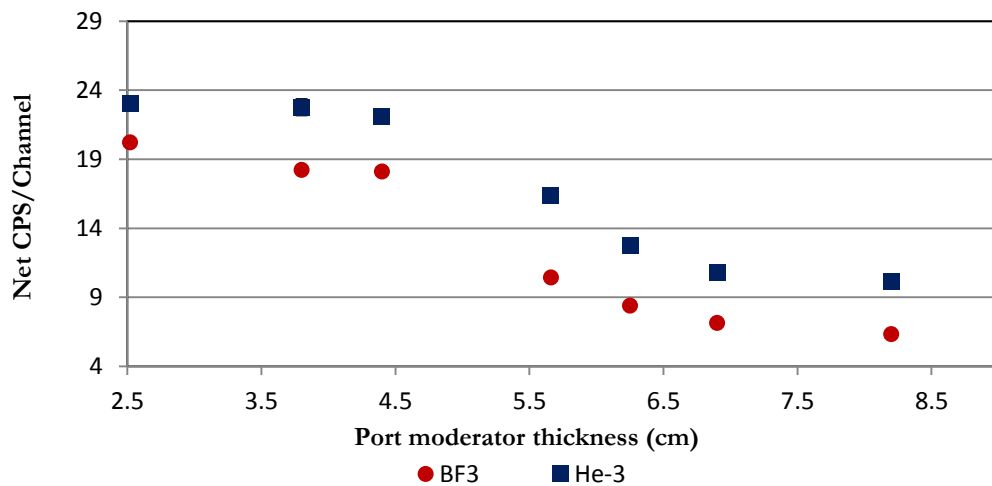


Figure 24: Experimental Net Counts in He-3 and BF3 Detectors at Different HDPE Port Moderator Thicknesses, Generator Power (2800 W).

Figure 25, Figure 26 and Figure 27 show He-3 and B-lined NaI detector response at different neutron generator power and at varying distances from the edge of the neutrons port. The count rate in both detectors decreases as the detectors are moved further from the port and also as the neutron generator power decreases, (thereby decreasing the neutron flux). Higher neutron detection efficiency is shown for the boron-lined NaI detector compared to He-3 detector which validates the simulation results from MCNP. Detailed results found in Table 12, Appendix C. Standard deviation is less than 4%.

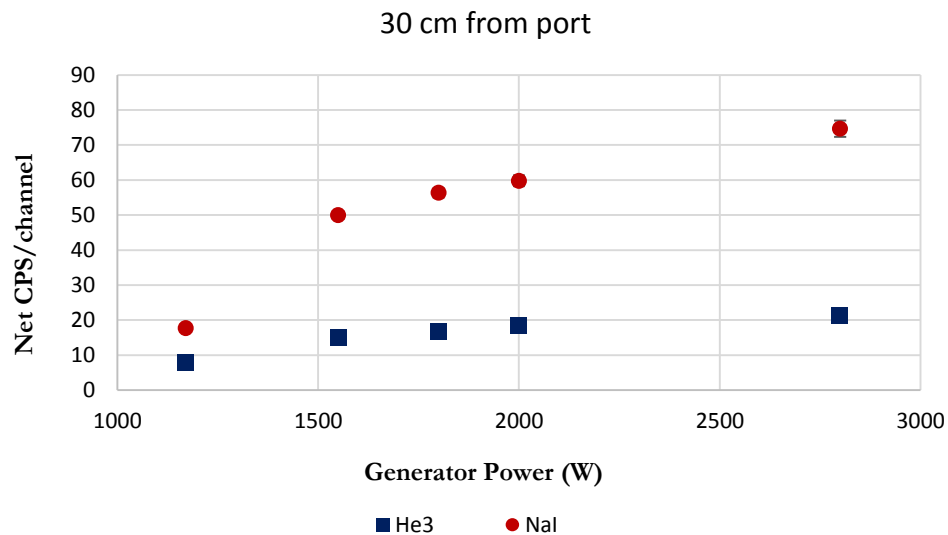


Figure 25: Detector Response of B-lined NaI and He-3 detectors at Varying Neutron Generator Power and Fixed Distance at 30 cm from Port.

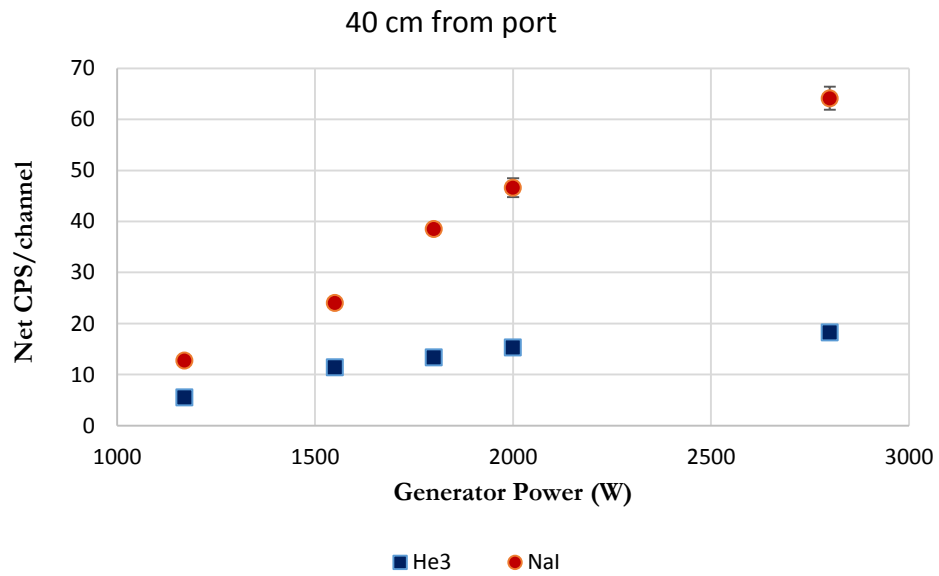


Figure 26: Detector Response of B-lined NaI and He-3 detectors at Varying Neutron Generator Power and Fixed Distance at 40 cm from Port.

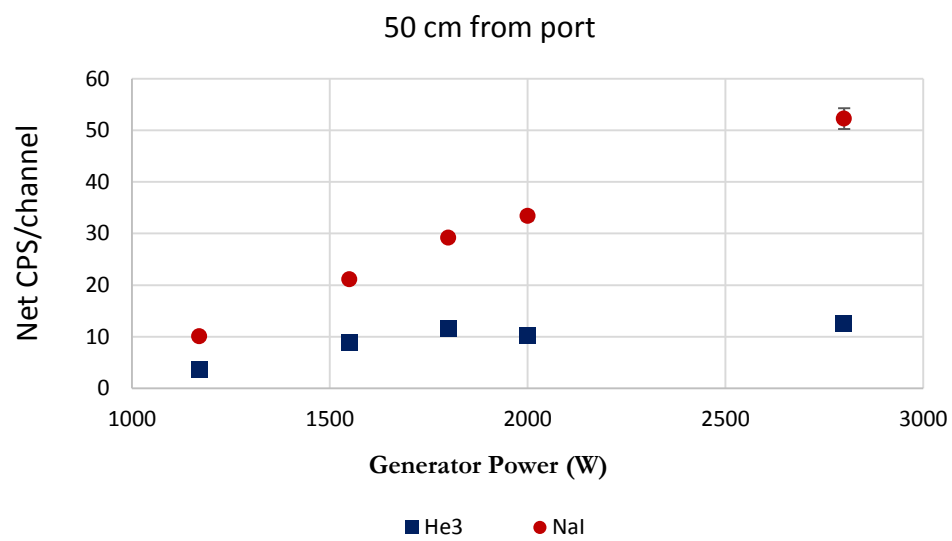


Figure 27: Detector Response of B-lined NaI and He-3 Detectors at Varying Neutron Generator Power and Fixed Distance at 50 cm from Port.

Figure 28, Figure 29 and Figure 30 show response of He-3 and BF3 detectors at different neutron generator power and at varying distances from the neutrons port. It can be seen that the count rate in both detectors decreases as the detectors are moved further from the port and also as the neutron generator power decreases, (thereby decreasing the neutron flux). As expected, higher neutron detection efficiency is shown for the He-3 detector than BF3 detector at all powers and all distances from the port. Detailed results can be found in Table 13, Appendix C. Standard deviation is less than 4%.

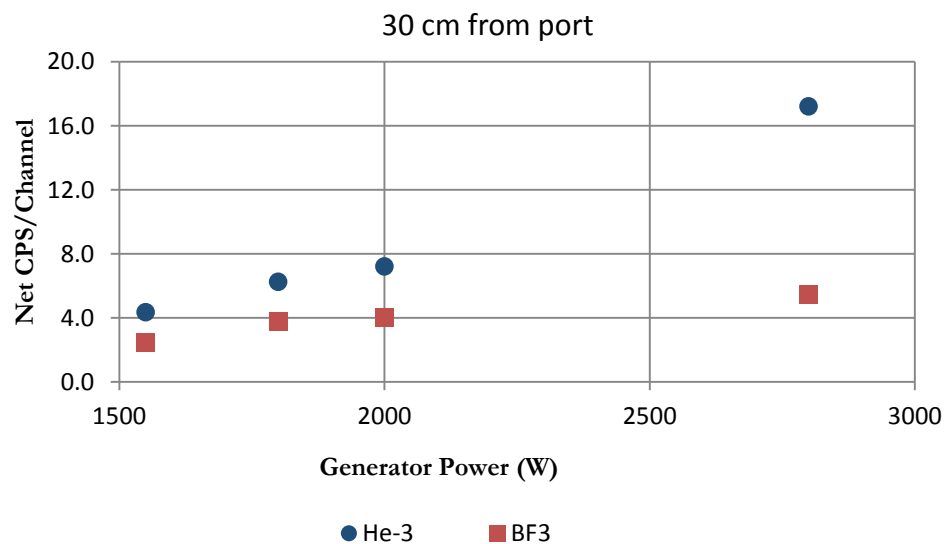


Figure 28: Response of He-3 and Bf3 detectors at Varying Neutron Generator Power and at 30 cm from port.

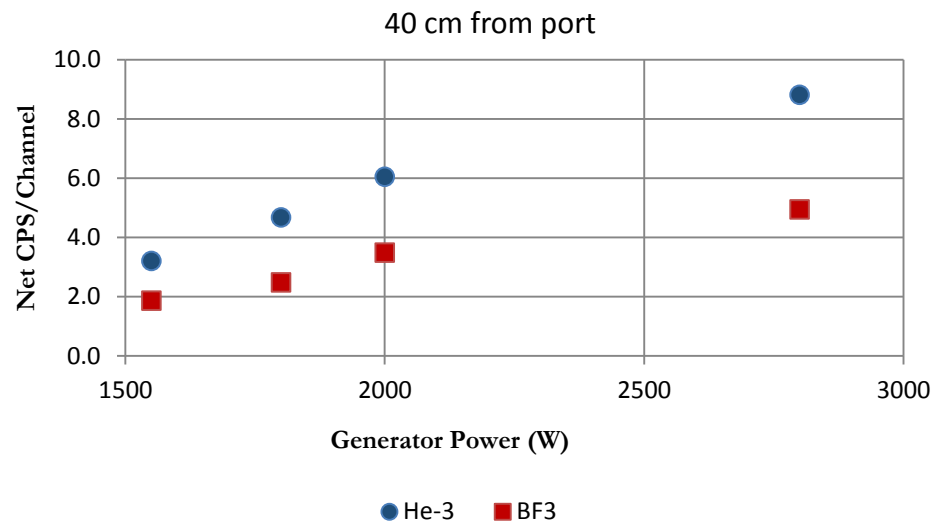


Figure 29: Response of He-3 and BF3 Detectors at Varying Neutron Generator Power and at 40 cm from Port.

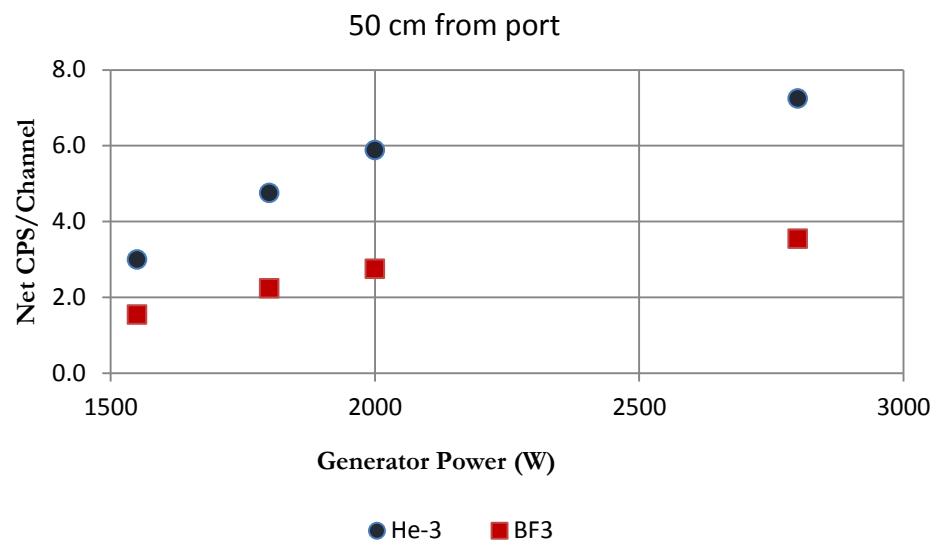


Figure 30: Response of He-3 and Bf3 Detectors at Varying Neutron Generator Power and at 50 cm from Port.

Chapter 4: Conclusions

B-lined NaI as an alternate neutron detector has been compared to BF₃ and scarce He-3 detectors. MCNP simulations and experimental measurements were used to calculate the neutron response in various neutron flux distributions emitted from D-D neutron generator. The results show a good sensitivity to changes in neutrons flux distributions, and a higher efficiency of B-lined NaI than that of He-3 and BF₃ detectors used in this work despite of the smaller volume of NaI detector used. An added benefit is the ability of the detector assembly to provide information about the gamma rays from the sample and surrounding medium. The results show that the boron-lined NaI is a good alternative and can replace the scarce and very expensive He-3 detector. The efficiency of the boron-lined neutron detector can be further improved by using enriched boron-10 layer. More work is needed on understanding the response of BF₃. More investigations on the response of boron-lined NaI detector are recommended using other neutron sources like ²⁵²Cf and Am/Be as a goal to use it in RPMs.

References

- [1] Tsoulfanidis, Nicholas. Measurement and detection of radiation. CRC press, 2010.
- [2] Kramer, David. "DOE begins rationing helium-3." *Physics Today* 63.6 (2010):22.
- [3] Isotopes, Managing Critical. "Weaknesses In DOE's Management Of Helium-3 Delayed The Federal Response To A Critical Supply Shortage." US Government Accountability Office GAO-11-472. (Sept. 2011).
- [4] Bentz, J., et al. "US Government Approach to Addressing the 3 He Shortage." *AAAS workshop on*. Vol. 3. 2010.
- [5] Glenn Knoll, Radiation Detection and Measurement, John Wiley and Sons, New York, USA, 2010.
- [6] Simpson, A. P., et al. "A review of neutron detection technology alternatives to helium-3 for safeguards applications." INMM 52nd Annual Meeting. Vol. 8. 2011.
- [7] Kouzes, Richard T., et al. "Neutron detection alternatives to 3He for national security applications." *Nuclear Instruments and Methods in Physics Research Section A: Accelerators, Spectrometers, Detectors and Associated Equipment* 623.3 (2010): 1035-1045.
- [8] Ely, James H., et al. Modeling and simulation optimization and feasibility studies for the neutron detection without helium-3 project. No. PNNL-22228. Pacific Northwest National Laboratory (PNNL), Richland, WA (US), 2013.
- [9] Urffer, Matthew J. "Design of a Neutron Detector Capable of Replacing He-3 Detectors Utilizing Thin Polymeric Films." (2012).
- [10] Kouzes, Richard T., and James H. Ely. Lithium and Zinc Sulfide Coated Plastic Neutron Detector Test. No. PNNL-19566. Pacific Northwest National Laboratory (PNNL), Richland, WA (US), 2010.
- [11] Metwally, Walid A. "Existing NaI detectors; an efficient alternative to He-3 detectors." *Nuclear Instruments and Methods in Physics Research Section B: Beam Interactions with Materials and Atoms* 338 (2014): 48-51.
- [12] Kouzes, Richard T., et al. "Alternatives to 3He for neutron detection for homeland security." Pacific Northwest National Laboratory Report (2010).
- [13] Doan, Tri C. Cao. Thermal neutron detector based on hexagonal boron nitride. Diss. 2016.

- [14] Koontz, P. G., George Robert Keepin, and J. E. Ashley. "ZnS (Ag) phosphor mixtures for neutron scintillation counting." *Review of Scientific Instruments* 26.4 (1955): 352-356.
- [15] Guzmán-García, Karen A., et al. "Study of a $^{10}\text{B} + \text{ZnS (Ag)}$ neutron detector as an alternative to ^3He -based detectors in Homeland Security." *Applied Radiation and Isotopes* 117 (2016): 58-64.
- [16] Lintereur, Azaree T., et al. Boron-lined neutron detector measurements. No. PNNL-18938 Rev 1. Pacific Northwest National Laboratory (PNNL), Richland, WA (US), 2010.
- [17] Walker, Scottie. Spectrally-matched neutron detectors designed using computational adjoint $S \ll N$ for plug-in replacement of Helium-3. Diss. Georgia Institute of Technology, 2013. Retrieved from <https://www.osti.gov/scitech/servlets/purl/1111077>
- [18] Lintereur, Azaree T. Neutron Multiplicity Counter Design Without Helium-3. Diss. University of Florida, 2013. Retrieved from http://ufdcimages.uflib.ufl.edu/UF/E0/04/59/06/00001/LINTEREUR_A.pdf
- [19] Okowita, Alexander Martin. "Characterization of Lithium-6 as a Commercial Helium-3 Alternative for Nuclear Safeguards and Security." (2014).. Retrieved from http://trace.tennessee.edu/utk_gradthes/3166
- [20] Vainionpää, J. H., et al. "Technology and applications of neutron generators developed by Adelphi Technology, Inc." *Physics Procedia* 60 (2014): 203-211.
- [21] Moderated and Shielded Neutron Generators for Safe Laboratory Use (2015, July). Retrieved from <http://www.adelphitech.com/products/moderated-and-shielded.html>
- [22] X-5 Monte Carlo Team, MCNP – A General Monte Carlo N-Particle Transport Code, Version 5, University of California, Los Alamos National Laboratory, 2003.
- [23] Brown, Forrest B., and Yasunobu Nagaya. The MCNP5 random number generator. No. LA-UR-02-3782. Los Alamos National Laboratory, 2002.
- [24] X 5 Monte Carlo team. MCNP—a general Monte Carlo n-particle transport code, version 5, Vol. II: Users Guide. LANL Report LA CP 03 0245 (Los Alamos National Laboratory, Los Alamos, NM) (April 2003 revised June 2004).
- [25] Monte Carlo Team, MCNP – A General Monte Carlo N-Particle Transport Code, Version 6, University of California, Los Alamos National Laboratory, 2012.

- [26] MedCalc Software. (Digimizer Version 4.6.1).(2016). Retrieved from <https://www.digimizer.com>
- [27] McConn, Ronald J., et al. Compendium of material composition data for radiation transport modeling. No. PNNL-15870 Rev. 1. Pacific Northwest National Laboratory (PNNL), Richland, WA (US), 2011.
- [28] "Basic Physics of Nuclear Medicine/Scintillation Detectors." *Wikibooks, The Free Textbook Project*. 25 Feb 2018, 21:28 UTC. 29 Apr 2018, 19:48 <https://en.wikibooks.org/w/index.php?title=Basic_Physics_of_Nuclear_Medicine/Scintillation_Detectors&oldid=3378449>.
- [29] Castro, Vinícius A., et al. "MCNP to study the BF3 detection efficiency." INAC, Rio de Janeiro (2011).

List of Publications

Metwally, Walid A., and Emam, Amira G. "Experimental validation and testing of a NaI boron-lined neutron detector." Nuclear Instruments and Methods in Physics Research Section B: Beam Interactions with Materials and Atoms 422 (2018): 7-11.

Appendix A: MCNP6 input file

```

c ##### B-lined NaI vs. He-3 detectors #####
c ----- front port with 1.28 cm HDPE , 2 detectors at distance 30 cm in front of detector-
c -----center of effective volume of both detectors 30 cm to right of edge of front port
c cell cards

10  4 -0.001205 -17 1      $ space^^ at handles
20  1  -2.7 -1 2 13      $ 0.3 Al layer out
30  2 -11.35 -2 3 13      $ 1.3 lead out
40  1  -2.7 -3 4 16 13    $ 0.3 Al out
50  3 -1.08 -1 -4 5 16 21 13  $ Borated poly ethylene out
60  4 -0.001205 -5 6 13    $ space around shielding
70  1  -2.7 -6 7 21 13    $ lead inn
90  1  -2.7 -8 9 13 14 21 13  $ inner Al inn
100 9  -0.96 -9 10 13 14 21 15  $ HDPE around cylinder
102 4 -0.001205 -19 558 559 560  $ central cylinder (Air)
104 4 -0.001205 -13      $ front port
105 9  -0.96 -14      $ HDPE sample plug left DD
106 9  -0.96 -1 -15      $ HDPE front port moderator
107 3  -1.08 -1 -16      $ Borpoly sample plug left
108 9  -0.96 -18 17 13    $ HDPE outer shielding
109 4 -0.001205 -31 18 24 28 (-18.6 ) $ outside Air of shielding
110 5  -8.03 -10 19 558 559 560  $ St. Steel layer around cylinder
112 4 -0.001205 -21      $ space for vacuum pump
113 6  -2.25 (-22 30 -31 )    $ ground
122 0      (31 :-30 )    $ outer world

c ----- V-Shape source geometry-----

549 17  -8.96 -558  $ Upper V Sour
560 4 -0.001205 -560  $ Upper V Sour
550 17  -8.96 -559  $ Lower V Sour

c -----
c

```

115 7 -2.34 -24 25 \$ Natural B layer of NaI detector

116 1 -2.7 -25 26 \$ Al casing of NaI detector

117 8 -3.67 -26 \$ NaI detector

119 5 -8.03 -28 29 \$ stainless steel casing of He-3

120 10 -0.000497 -29 \$ He-3 active material

c surface cards

c ----- Shielding and body of generator -----

1 rpp -74.32 79.35 -36.515 36.515 -36.515 36.255

2 rpp -74.02 79.05 -36.215 36.215 -36.215 35.955

3 rpp -72.72 77.75 -34.915 34.915 -34.915 34.655

4 rpp -72.42 77.45 -34.615 34.615 -34.615 34.355

5 rpp -57.18 61.89 -24.455 24.455 -24.355 24.355

6 rpp -34.94 18.09 -23.81 23.81 -24.355 24.355

7 rpp -34.64 17.79 -23.51 23.51 -24.055 24.055

8 rpp -33.34 16.49 -22.21 22.21 -22.755 22.755

9 rpp -33.04 16.19 -21.91 21.91 -22.455 22.455

c -----inside generator -----

10 rcc 16.19 0 0 -49.23 0 0 7.6 \$ central cylinder

c ----- to close top port add c to surfaces 11 , 12

c 11 rcc 0 0 13.7 0 0 41.895 6.4 \$ HDPE sample plug

c 12 rcc 0 0 24.355 0 0 11.9 7 \$ Borpoly sample plug top

13 rcc -16.8 -8.881 0 0 -42.874 0 6.4 \$ front port

14 rcc -16.8 7.601 0 0 14.21 0 6.4 \$ HDPE sample plug left DD

15 rcc -16.8 -7.601 0 0 -1.28 0 6.4 \$ HDPE front port moderator

16 rcc -16.8 24.455 0 0 10.182 0 7 \$ Borpoly sample plug left

17 rpp -74.32 79.35 -36.515 36.515 -51.755 40.355

18 rpp -89.56 94.59 -51.755 51.755 -51.755 55.595

19 rcc 16.19 0 0 -49.23 0 0 7

21 rpp -32.83 -16.784 -11.303 11.303 -34.615 -7.7 \$ space for vacuum pump

22 pz -51.755 \$ ground surface

```

30    pz -81.755      $ ground surface lower
31    so 1000         $ outer world

c ----- Source geometry -----

558  50 rpp -4.699 4.699 -2.857 2.857 0 1.27  $ Upper copper
560  50 rpp -4.69 4.69 -2.85 2.85 -0.001 0
559  60 rpp -4.699 4.699 -2.857 2.857 -1.27 0  $ Lower copper
561  50 pz -0.0015

c ----- Detectors -----

24    rcc 12.75 -81.755 -10 13.7 0 0 3.22      $ B-layer of NaI detec
25    rcc 12.75 -81.755 -10 13.7 0 0 3.02      $ Al casing of NaI det
26    rcc 13.25 -81.755 -10 12.7 0 0 2.52      $ NaI detector
28    rcc 4.055 -81.755 10 31.09 0 0 2.54      $ st.steel(31.09)of He3
29    rcc 4.105 -81.755 10 30.99 0 0 2.49      $ He-3 detector (30.99 cm)

c Data cards

mode n p

c ----- Materials-----

m1    13027.         -1    $ Al
m2    82000.         -1    $ lead
m3    6000.         -0.813466  $Borated polyethylene
      1001.         -0.136534 5010.    -0.0092155 5011.    -0.0407845
m4    6000.         -0.000125  $Air
      7014.         -0.6869 8016.    -0.301248 18000.    -0.011717
m5    24000.         -0.18    $Stainless steel 304 PNNL page 288
      28000.         -0.08 26000.    -0.74
c ----- Ground $ concrete MCNP -----PNNL page 95
m6    1001.         -0.00453
      8016.         -0.5126 11023.    -0.01527 13027.    -0.03555
      14000.        -0.36036 20000.    -0.05791 26000.    -0.01378
c ----- HDPE (thick plastic sample) & Polyethylene non borated PNNL page 239
m9    1001.         -0.143716  $ Hydrogen
      6000.         -0.856284

```

```

m17 29000.      -1  $Copper

c -----Natural Boron-----

m7  5010.      -0.199  5011.      -0.801

c ----- Sodium Iodide -----

m8  11023.     -0.153373  53127.     -0.846627

c ----- He-3 -----

m10 2003.      -1 $ He-3

c -----new code-----

*tr50 0 0 0.655 8 90 82 90 0 90 98 90 8

*tr60 0 0 -0.655 352 90 262 90 0 90 82 90 8

c ----- Importance -----

imp:n 1 19r    0      1 7r      $ 10, 120

imp:p 1 19r    0      1 7r      $ 10, 120

c -----

mt3  poly.10t

mt9  poly.10t

c ----- TALLIES-----

c ----- NaI detector -----

f4:n 115      $ neutrons flux in B layer

e4: 0 1000i 2.45  $ Neutrons .energy binning

f8:p 117      $ photon tally at NaI detector

e8: 0 1024i 10   $ photon energy binning

c -----

c ----- He-3 Detector -----

f14:n 120      $ neutron flux at He-3 detector

fm14 (-1 10 103)  $ tally multiplier for np reaction

c -----

c -----source-----

sdef  ERG=2.45  x=d1 y=d2 z=d3 tr= d4  $ source on both surfaces

si1 -4.6 4.6

c  sp1 0 1.0

si2 -2.857 2.857

```

```
sp2 0 1.0
```

```
si3 L -0.01 0.01
```

```
sp3 1 1
```

```
si4 L 50 60
```

```
sp4 1 1
```

```
c DS4 L 50 60
```

```
c -----
```

```
phys:p
```

```
print
```

```
nps 2000000000
```

Appendix B: Simulation Results

Table 9: Photon Counts per Source Particles at Region of Interest from MCNP Simulation for NaI Detector with and without Boron Layer.

photon Energy (MeV)	With Boron			No Boron		
	CPSP	Sigma	Sigma %	CPSP	Sigma	Sigma %
0.34146	5.31E-07	3.44E-08	6.47	5.51E-07	3.50E-08	6.35
0.35122	5.31E-07	3.44E-08	6.47	5.42E-07	3.47E-08	6.4
0.36098	5.58E-07	3.52E-08	6.31	5.69E-07	3.56E-08	6.25
0.37073	5.69E-07	3.56E-08	6.25	5.67E-07	3.55E-08	6.26
0.38049	5.4E-07	3.47E-08	6.42	5.49E-07	3.49E-08	6.36
0.39024	4.71E-07	3.24E-08	6.87	4.73E-07	3.24E-08	6.85
0.4000	4.64E-07	3.21E-08	6.92	4.56E-07	3.18E-08	6.98
0.40976	3.84E-07	2.92E-08	7.60	3.91E-07	2.95E-08	7.54
0.41951	4.38E-07	3.12E-08	7.12	4.36E-07	3.11E-08	7.14
0.42927	4.27E-07	3.08E-08	7.22	4.16E-07	3.04E-08	7.31
0.43902	3.89E-07	2.94E-08	7.56	3.78E-07	2.90E-08	7.67
0.44878	3.69E-07	2.86E-08	7.76	3.73E-07	2.88E-08	7.72
0.45854	3.82E-07	2.91E-08	7.62	4.04E-07	3.00E-08	7.41
0.46829	3.78E-07	2.9E-08	7.67	3.67E-07	2.85E-08	7.78
0.47805	1.39E-06	5.56E-08	3.99	8.40E-07	4.32E-08	5.14
0.4878	3.73E-07	2.88E-08	7.72	3.60E-07	2.83E-08	7.86
0.49756	2.93E-07	2.55E-08	8.70	2.96E-07	2.56E-08	8.67
0.50732	3.22E-07	2.67E-08	8.30	3.36E-07	2.73E-08	8.14
0.51707	6.98E-07	3.94E-08	5.64	7.24E-07	4.01E-08	5.54
0.52683	2.58E-07	2.39E-08	9.28	2.73E-07	2.47E-08	9.02
0.53659	2.53E-07	2.37E-08	9.37	2.53E-07	2.37E-08	9.37
0.54634	2.24E-07	2.23E-08	9.95	2.29E-07	2.25E-08	9.85
0.55610	2.78E-07	2.48E-08	8.94	2.87E-07	2.52E-08	8.8
0.56585	2.53E-07	2.37E-08	9.37	2.47E-07	2.34E-08	9.49
0.57561	1.71E-07	1.95E-08	11.40	1.73E-07	1.96E-08	9.32
0.58537	2.2E-07	2.21E-08	10.05	2.24E-07	2.23E-08	9.95
0.59512	2.51E-07	2.36E-08	9.41	2.64E-07	2.42E-08	9.17
0.60488	1.98E-07	2.1E-08	10.60	2.02E-07	2.12E-08	9.48

Appendix C: Experimental Results

Table 10: Experimental Response of He-3 and B-lined NaI Detectors at Various HDPE Moderator Thicknesses.

Port Thickness (cm)	He-3 Detector			B-lined NaI Detector		
	Net CPS/channel	Sigma	Sigma %	Net CPS/channel	Sigma	Sigma %
1.28	14.495	0.109	0.75	16.673	0.377	2.26
1.91	12.330	0.109	0.88	15.946	0.3161	1.98
2.52	10.462	0.076	0.72	13.777	0.2428	1.76
4.40	9.5762	0.062	0.65	11.890	0.2168	1.82
6.19	6.2813	0.045	0.72	8.813	0.213	2.41
7.44	4.771	0.033	0.69	8.011	0.195	2.44
10.36	3.800	0.029	0.79	6.616	0.215	3.24
11.80	3.596	0.030	0.85	5.751	0.214	3.72
13.09	2.901	0.026	0.88	5.593	0.220	3.93

Table 11: Experimental Neutron Response of BF3 and He-3 Detectors at Different HDPE Moderator Thicknesses.

Port Thickness (cm)	He-3 Detector			BF3 Detector		
	Net CPS/channel	Sigma	Sigma %	Net CPS/channel	Sigma	Sigma %
2.52	23.0003	0.490	2.13	20.2097	0.2156	1.07
3.80	22.7727	0.589	2.59	18.2207	0.2363	1.30
4.40	22.1219	0.360	1.63	18.1148	0.2155	1.19
5.66	16.367	0.174	1.06	10.4271	0.129	1.24
6.25	12.7224	0.117	0.92	8.3961	0.1045	1.24
6.90	10.8024	0.128	1.18	7.1444	0.075	1.05
8.20	10.1447	0.144	1.42	6.3383	0.090	1.42

Table 12: Experimental Neutron Response of B-Lined NaI and He-3 Detectors at Various Powers and Shifts.

Power (W)	Distance from port (cm)	He-3 Detector			B-lined NaI Detector		
		Net CPS/channel	Sigma	Sigma %	Net CPS/channel	Sigma	Sigma %
1170	30	7.691	0.1146	1.490	17.696	0.5258	2.971
1170	40	5.561	0.1214	2.183	12.765	0.4824	3.779
1170	50	3.642	0.0560	1.538	10.053	0.3027	3.011
1550	30	15.123	0.2924	1.933	49.951	0.9870	1.976
1550	40	11.438	0.1764	1.542	24.034	0.8788	3.656
1550	50	8.855	0.0946	1.068	21.124	0.4661	2.207
1800	30	16.694	0.2582	1.547	56.343	1.3893	2.466
1800	40	13.352	0.1519	1.138	38.546	1.1631	3.017
1800	50	11.511	0.1199	1.042	29.207	0.6639	2.273
2000	30	18.515	0.2768	1.495	59.797	1.5231	2.547
2000	40	15.304	0.4060	2.653	46.635	1.8585	3.985
2000	50	10.140	0.1684	1.661	33.408	0.9079	2.718
2800	30	21.215	0.4323	2.038	74.666	2.2968	3.076
2800	40	18.274	0.3789	2.073	64.134	2.2496	3.508
2800	50	12.522	0.2617	2.090	52.241	2.0248	3.876

Table 13: Experimental Neutron Response of BF₃ and He-3 Detectors at Various Generator Powers and Distances from Port.

Power (W)	Distance from port (cm)	He-3 Detector			BF ₃ Detector		
		Net CPS/ channel	Sigma	Sigma %	Net CPS/ channel	Sigma	Sigma %
1550	30	4.337	0.063	1.460	2.456	0.040	1.640
1550	40	3.202	0.068	2.129	1.864	0.031	1.653
1550	50	2.997	0.054	1.805	1.544	0.028	1.792
1800	30	6.241	0.129	2.074	3.752	0.048	1.281
1800	40	4.672	0.085	1.823	2.477	0.041	1.647
1800	50	4.752	0.074	1.561	2.229	0.035	1.569
2000	30	7.197	0.179	2.484	3.979	0.046	1.166
2000	40	6.043	0.117	1.941	3.488	0.063	1.794
2000	50	5.885	0.054	0.922	2.751	0.034	1.223
2800	30	17.199	0.249	1.447	5.461	0.064	1.176
2800	40	8.814	0.202	2.297	4.945	0.086	1.742
2800	50	7.243	0.104	1.439	3.542	0.055	1.551